SEP. - DEC. 2022 ● Volume XXIII Number

# THE ASEAN JOURNAL OF RADIOLOGY

## Highlight

- Original Article
- ASEAN Movement in Radiology

Official Journal of

Radiological Society of Thailand

The Royal College of Radiologists of Thailand

ASEAN Association of Radiology

Foundation for Orphan and Rare Lung Disease

ASEAN
JOURNAL OF RADIOLOGY

ISSN 2672-9393

# The ASEAN
## Journal of Radiology

# CONTENTS

THE ASEAN JOURNAL OF RADIOLOGY
ISSN 2672-9393

From The Editor

# The first examination for professional license in medical physics in Thailand

Received 22 December 2022 ; accepted 22 December 2022
doi:10.46475/aseanjr.v23i3.201

COVID-19 infections in Thailand appear to be on the rise again, especially among those who are unvaccinated or not fully vaccinated. Fatalities were mostly observed among the elderly or those with underlying health complaints. At the end of November, the BA.2.75 sub-variant of COVID-19 already accounted for as much as 58% of COVID-19 cases in the country. From January 1st to October 3rd, 2,488,093 COVID-19 infections were recorded, of which 11,587 died [1]. The number was equal to the mortality rate of less than 0.5% in general. More people have been infected or developed familiarity with living with infected familial members or friends. The atmosphere in business, tourism and service sectors became almost the same as in pre-pandemic years. Thailand's Public Health Minister is confident that COVID-19 infections during the New Year celebrations will be kept under control.

The concern that the monkeypox outbreak will have a high chance of being prolonged in the same manner of HIV, despite not being as widespread as COVID-19, is relieved as there has been no report after the 12th case in October [2].

The Medical Council of Thailand, along with 16 other medical organisations including the Royal College of Radiologists of Thailand, have signed a petition seeking to limit the use of cannabis to medical purposes and firmly opposing its use for recreational purposes. Concerning negative consequences and feasible dangers from illegal canabis that the current policies fail to consider allowing people to recklessly grow and use cannabis for treatment by themselves, five suggestions were held fourth as follows [3]:

- The use of cannabis for medical treatment must be based on empirical evidence.
- Cannabis must be of high quality and must be used under Thailand's Drugs Act, to protect patients who are treated with such plants. Any cannabis or its extracts used for treatment must not contain any contaminants.
- Doctors and pharmacists must be trained on how to use cannabis and its extracts.
- All patients must be screened and evaluated before, during and after treatment with cannabis.
- Government authorities, such as the Thai Food and Drug Administration, should also regulate the use of cannabis for medical purposes.

Even though the Ministry of Health announced on November 2nd, 2020 that profession license was required to practice medical physics in Thailand, the first license examination eventually took place on July 26th, 2022 under supervision of the Royal College of Radiologists of Thailand. The first seventeen medical physicists were licenced by the Department of Health Service Support on August 10th, 2022 [3]. It is strongly believed that this important step will lead to safer and better qualified practice and patients' care in Radiology.

THE ASEAN JOURNAL OF RADIOLOGY
ISSN 2672-9393

*Above: The first examination for professional licence in medical physics was organized by Department of Health Service Support, the Ministry of Health, under supervision of the Royal College of Radiologists of Thailand. Below: The first 17 licenced medical physicists in Thailand.*

*Wiwatana Tanomkiat, M.D.*
Editor,
The ASEAN Journal of Radiology
**Email:** aseanjournalradiology@gmail.com

## References

1. Thai PBS World [Internet]. Bangkok: TPBS; c2018 [cited 2022 Dec 22]. Thailand's COVID death toll rises, hospitalisations fall during past week. Available from: https://www.thaipbsworld.com/thailands-covid-death-toll-rises-hospitalisations-fall-during-past-week/

2. กรมควบคุมโรค. กระทรวงสาธารณสุข [อินเทอร์เน็ต]. นนทบุรี: กระทรวง; c2022 [[เข้าถึงเมื่อ 22 ธันวาคม 2565]. โรคติดเชื้อฝีดาษวานร(Monkeypox). เข้าถึงได้จาก:https://ddc.moph.go.th/monkeypox/index.php

3. ข้อเสนอเกี่ยวกับนโยบายกัญชาของประเทศไทย [อินเทอร์เน็ต]. [เข้าถึงเมื่อ 22 ธันวาคม 2565]. เข้าถึงได้จาก: https://tmc.or.th/pdf/tmc-cannabis-1-160965.pdf

THE ASEAN JOURNAL OF RADIOLOGY
ISSN 2672-9393

Original Article

# Associated ultrasound findings improve the accuracy of twinkling artifacts in kidney stone diagnosis

*Rujiluck Rojthamrong, M.D.*[(1) (2)]
*Kewalee Sasiwimonphan, M.D.*[(1) (2)]
From [(1)]Department of Radiology, Faculty of Medicine, Chulalongkorn University,
[(2)]King Chulalongkorn Memorial Hospital the Red Cross Society, 1873 Rama IV Road, Pathumwan, Bangkok, Thailand.
Address correspondence to K.S. (e-mail: kewalees@gmail.com)

Received 28 September 2022; revised 24 November 2022; accepted 26 November 2022
doi:10.46475/aseanjr.v23i3.189

## Abstract

**Background:** Twinkling artifact (TA) in color Doppler ultrasound is commonly used as a sign of kidney tract stone detection but the accuracy is limited as compared with unenhanced computed tomography (CT).

**Objective:** Define the associated ultrasound findings that may improve the accuracy of TA compared with CT for diagnosing kidney stones.

**Materials and Methods:** Prospective study was conducted on 128 TAs in patients sent for unenhanced CT KUB and performed color Doppler ultrasound on the same day. TA sizes and associated sonographic signs were recorded and analyzed with receiver operating characteristic curves (ROCs). The diagnostic reference was the CT scan.

**Results:** There was a total of 128 TAs with the size of 3.95 mm (2.7-6 mm). Only 30 TAs showed as kidney stones in CT. The sizes of kidney stones in CT were 5.4 mm (3.4-6.4 mm) which represented a significant difference in TA size ($P$ = 0.002). ROC curve analysis showed that 5 mm would be the optimal size of TA for kidney stone predictions. Other significant signs for improved diagnosis include echoic foci ($P$ = 0.039), posterior shadows ($P$ = 0.001), long TA tails ($P$ = 0.001) and 2$^{nd}$ approach TA ($P$ = 0.001). Then a predictive AT model was created to predict kidney stones, which moderately improved diagnosis accuracy for kidney stones with good agreement.

**Conclusion:** The combination of TA and other sonographic signs are moderately associated with kidney stone diagnosis including TA size (> 5 mm), posterior acoustic shadow, long TA tail, junctional line location and focal Caliectasis.

**Keywords:** Twinkling artifact, Color doppler ultrasound, Kidney stones, Renal calculi.

## Introduction

Kidney stones are one of the most frequent concerns of people referred to emergency centers, with an occurrence likelihood of 12% for males and 6% for females [1]. Ultrasound (US) and computed tomography (CT) scans are widely used as imaging modalities to diagnose the disease [2]. CT scans without intravenous contrast administration are widely accepted as the reference standard imaging technique to confirm or deny the diagnosis of urinary calculi. Despite the high sensitivity and specificity values of CT, the cost-effectiveness ratio, high radiation doses and motion artifact disadvantages of this application warrant the development of alternative methods with similar reliability.

THE ASEAN JOURNAL OF RADIOLOGY
ISSN 2672-9393

Recently, there has been growing awareness of the overuse of CT and the associated radiation effects arising from the evaluation of patients with acute flank pain [3]. The development of US probe technologies and US imaging techniques has improved the sonographic image quality and enhanced the utility of US in diagnosing urinary tract calculi.

In 1996, Rahmouni et al. [4] defined a "twinkling" artifact as a color Doppler (CD) artifact generated by a strongly reflecting medium: [4] the result was a rapidly changing mixture of red and blue color signals arising from a point behind a stationary object, which represents a substantial improvement for the sonographic detection of stones [5-6]. The TA on color Doppler US could be a good and safe alternative imaging modality with results comparable to those from noncontrast-enhanced CT for the sensitive detection of urolithiasis <5 mm. The initial study showed that the sensitivity, accuracy, and positive predictive values of TA for the detection of calculus were 94%, 94%, and 100%, respectively [7]. However, a study in 2016 found that isolated sonographic twinkling artifacts have a high false-positive rate (60%) for the diagnosis of renal calculi [8]. There are also conflicting results regarding the sensitivity and specificity of twinkling artifacts. Some studies have reported that the accuracy of the artifact depends on both the setting of the device and the shape of the stone. It has been argued that this artifact is also observed in many parts of the kidney where no stones exist [9].

In considering the size of the detected stone, Aytac and Ozcan [5] concluded in 1999 that TA helps differentiate a small stone from other small echogenic structures. Studies such as those of Yavuz et al. [10] and Hanafi et al. [7] have revealed that the TA has been a useful CDUS tool for detecting small urinary stones. However, Masch et al. [8] showed that an isolated TA has a high false-positive rate (60%) for the diagnosis of renal calculi in patients without known urolithiasis. The specificity and positive likelihood ratio for the diagnosis of renal calculi improved but declined in sensitivity when additional diagnostic features such as sonographic twinkling artifacts and echogenic foci were present. A limitation of this study was the retrospective design, which involved recruitment of the study population based on finalized abdominal ultrasound reports containing

the words "twinkle" or "twinkling" in reference to suspected urinary tract calculus; this delayed the collection of data between the index ultrasound and the reference standard CT in the study (mean delay of 8 days).

The sensitivity and specificity values from prior studies are still inconclusive. Most of the prior studies are retrospective studies that used small sample sizes and multiple confirmation methods, such as surgery, computed tomography or the collection of a stone extracted by the patient during micturition.

The associated ultrasound findings of the TA in CDUS compared to CT results for the evaluation of kidney stones have not been well established.

Our hypothesis was that associated findings with twinkling artifacts might have been significantly related to accuracy in kidney stone diagnosis. The purpose of our study is to assess the correlation between sonographic TA findings and CT results for the diagnosis of kidney stones.

Imaging findings of TAs associated with renal stones have been documented in the literature. In some cases, grayscale US simultaneously shows multiple findings, enabling confident diagnosis of stones. However, in some cases, grayscale US and CDUS findings are equivocal or inconclusive, but there is high clinical suspicion of renal disease. Because the diagnosis of stones from US is not always certain, a clear way of expressing the likelihood of renal stones is needed. This can be achieved by linking imaging findings of TA with scores categorizing imaging findings as positive, negative, or indeterminate for diagnosing renal stones.

In this study, we introduce a more systematic approach to use TA for the diagnosis of stones. This article represents a feasibility study of our standardized reporting format system using a cohort of patients who underwent CT of the abdomen within 6 hours before or after an US examination. We undertook this study to assess the diagnostic accuracy of the system and the usefulness of specific imaging findings, and to evaluate its reproducibility.

THE ASEAN JOURNAL OF RADIOLOGY
ISSN 2672-9393

## Materials and methods

### Patients

Ethics approval was provided by the institutional review board, the Faculty of Medicine, Chulalongkorn University, Bangkok, Thailand (No. 617-62). A written consent was obtained from all study participants. From August 2019 to September 2020, we prospectively studied patients in our hospital who were suspected of having kidney stones. Thereafter, 40 patients underwent a CT scan when the subsequent ultrasound was performed on the same day, which did not result in a known CT result at the time of the ultrasound.

### Sonographic technique

On the same day and after the CT scan, the patients directly underwent a limited sonographic scan of the kidneys (LOGIQ™ E9, GE Healthcare, Milwaukee, WI, USA). The examination was performed by two radiologists using a curved low-frequency probe (1-6 MHz), color frequency 2.5 MHz, Gain 60-70 and the focus zone is located below the suspicious lesion and a high pulse repetition frequency with which the machine's scale was greater than 60 cm/s [11]. The pulse repetition frequency is defined as the number of pulses sent per second. We used a high pulse repetition frequency (PRF) to exclude aliasing artifacts arising from small vessels. This is a key technical factor for identifying and documenting twinkling artifacts. The twinkling artifacts documented rapidly changing color mix immediately behind suspect focal lesions on Color Doppler ultrasound [4]. The radiologists in this study had 3 and 13 years of experience and were not aware of the CT findings at that time.

The kidneys were evaluated with both grayscale and color Doppler imaging. TAs were detected, and associated findings were observed. The area at the interface between the renal sinus and renal cortex was defined as the junctional line, and this is shown in Figure 1. The length of the TA was defined as the tail of the TA if it was longer than its width, as shown in Figure 2. Once a TA was found, it was again detected in different US approaches and was categorized as a 2$^{nd}$ approach TA.

The radiologists filled out a standardized form indicating factors such as size, location, presence or absence of the long tail of the TA, the presence of a posterior acoustic shadow, evidence of hydronephrosis, and areas of high echogenicity with associated shadowing on grayscale images.

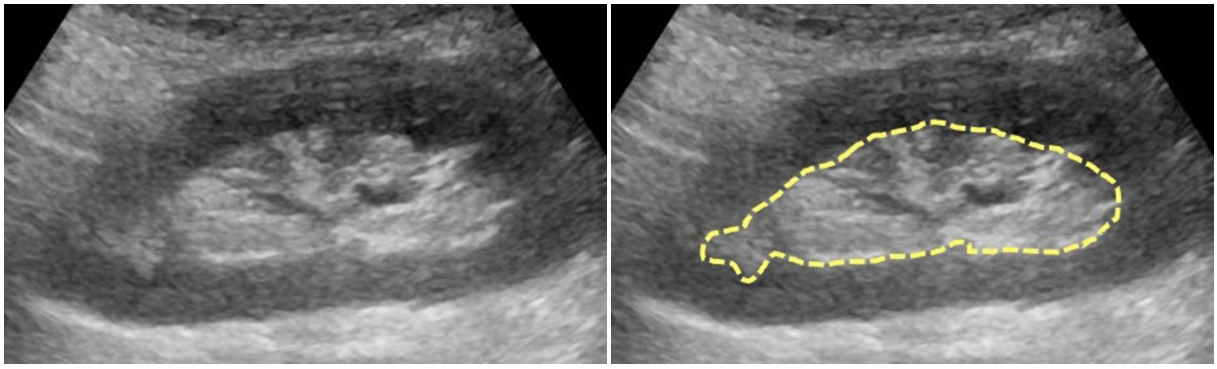

**Figure 1.** *Junctional line defined as the area of the interface between the renal sinus and renal cortex (dashed line).*

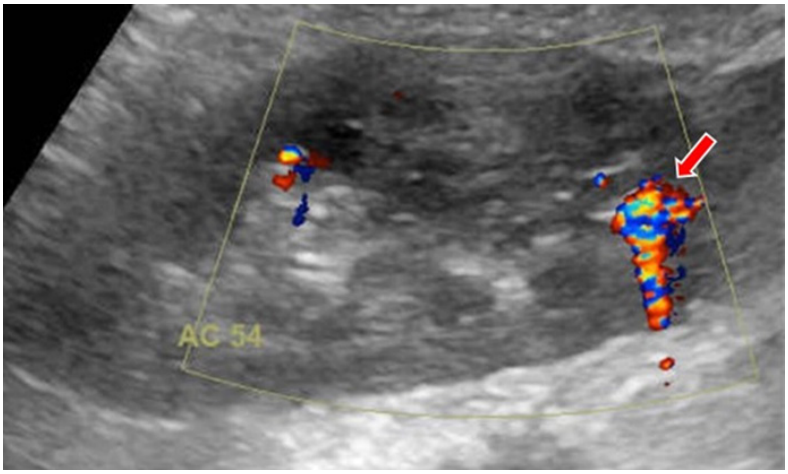


**Figure 2.** *TA image with a length longer than its width was defined as the tail of the TA (arrow).*

THE ASEAN JOURNAL OF RADIOLOGY
ISSN 2672-9393

**Computed tomography technique**

CT examinations were performed on MDCT scanners (Discovery CT 750 HDCT, GE Healthcare, Milwaukee, WI, USA) with a slice thickness/increment of 2.5/1.0 mm and a 120-kV tube potential. Tube current modulation was applied. Patients were scanned from the diaphragm to the pubic bone.

**Data analysis**

After independent evaluation of the CT scan and Doppler US of stones, the result of each imaging modalities were compared. The data were analyzed using STATA version 15.1. Continuous variables are presented as the mean ± SD or median (IQR) and n (%). Categorical data are reported as frequencies and proportions. P-values correspond to independent t tests or Mann-Whitney tests and chi-square tests. There was the AUC analysis defining the optimal cutoff size of the TA. Univariate and multivariate renal stones were evaluated using logistic regression analysis as well as model validation. The significance level was set at 0.05 for all statistical tests.

**Predictive model**

Our predictive model was based on a significant relationship existing between objective factors of the TA and a stone diagnosis in CT. The model consists of a scoring of imaging findings previously described to have an association with the presence or absence of kidney stones [5, 11, 13]. The objective imaging findings convey the radiologist's decision-making process to the clinician, and the final score reflects the corresponding implications for patient management.

## Results

A total of 128 TAs was identified and 46 TAs (35.9%) were found in male patients. The median size of the TAs was 3.95 mm (2.7 to 6 mm) in color Doppler US. There were only 30 TAs found as kidney stones in the CT scan. The median size of the renal stones was 5.4 mm (3.4 to 6.4 mm) in CT and 2.8 mm (2.3 to 6.6 mm) in color Doppler US. Echoic foci were detected in 84 TAs (65.6%). A posterior acoustic shadow was detected in 11 TAs (8.6%). The long tails and 2$^{nd}$ approach TA were detected in 65 (50.8%) and 108 (84.4%) TAs, respectively. A significant difference was found between the size of the TA and the presence of stones in CT ($P$ = 0.002). The table 1 described patients' characteristics in findings of TAs.

**Table 1.** *Characteristics of identified TAs (n=128).*

| Variable | n (%), mean ± SD, or medians with IQRs* |
|---|---|
| Male | 46 (35.9%) |
| BMI (ml/min/1.73 m$^2$) | 23.22 ± 3.4 |
| TA size (mm) | 3.95 (2.7-6) |
| Location: Cortex | 21(16.4) |
| Location: Junctional line | 72(56.3) |
| Location: Renal sinus | 35(27.3) |
| Echoic foci | 84(65.6) |
| Posterior acoustic shadow | 11(8.6) |
| Caliectasis | 7(5.5) |
| Stone size in CT | 4.5(3.4-6.4) |

**interquartile ranges*

THE ASEAN JOURNAL OF RADIOLOGY
ISSN 2672-9393

In Table 2 we describe the factors that significantly affected the accuracies of TA diagnoses, including echoic foci ($P$ = 0.039), posterior acoustic shadow ($P$ = 0.001), long TA tail ($P$ = 0.001), location at the junctional line (p=0.028), caliectasis (p=0.013) and 2nd approach TA ($P$ = 0.001). ROC curve analysis of the sizes of TAs (Figure 3) and the presence of stones in CT showed that 5 mm would be the optimal size for predicting renal stones. Additionally, the results showed that the location in the renal cortex was significantly related to no stone on CT scan and 35 TAs at the renal sinus indicated 10 stones that were confirmed with CT.

**Table 2.** *Associated findings that significantly supported the diagnosis of renal stones from TA findings (total n=128).*

| Stone-predicting factors | CT result positive (n=38) | CT result negative (n=90) | Odds ratio (95% CI) | p-value |
|---|---|---|---|---|
| TA Size (mm) | 5.45(3.3-6.6) | 3.5(2.4-4.8) | 1.19(1.04-1.37) | 0.01 |
| Longer tail of TA | 28(73.7%) | 37(41.1%) | 4.01(1.63-10.32) | 0.001 |
| Posterior acoustic shadow | 8(21.1%) | 3(3.3%) | 7.73(1.68-47.26) | 0.001 |
| Caliectasis | 5(13.2%) | 2(2.2%) | 6.67(1.01-71.97) | 0.013 |
| Echoic foci | 30(78.9%) | 54(60%) | 2.5(0.97-7) | 0.039 |
| Location at junctional line | 27(71.1%) | 45(50%) | 2.45(1.02-6.14) | 0.028 |
| Location at renal cortex | 1(2.6%) | 20(22%) | 0.09(0-0.65) | 0.006 |

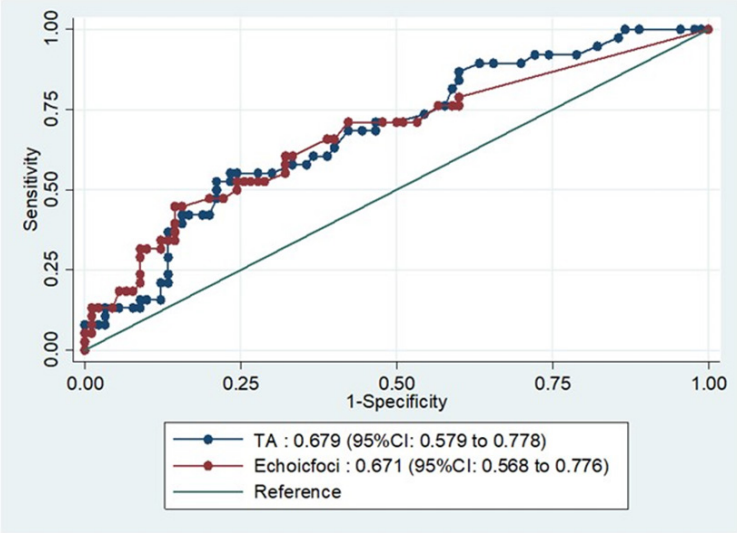


**Figure 3.** *Receiver operating characteristic (ROC) curves for the diagnosis of renal calculus by color Doppler TA and echoic foci. TA, AUC=0.679 (95% CI 0.579-0.778); echoic foci, AUC=0.671 (95% CI 0.568-0.776).*

The false positive ratio for TAs in our study was approximately 0.5, and the false positive ratios for locations at the junctional line, renal sinus and renal cortex were 0.5, 0.28, and 0.22, respectively. However, the high false positive rate for the location at the junctional line was accompanied by the highest sensitivity, approximately 0.71, as compared to approximately 0.26 and 0.03 for the renal sinus and renal cortex, respectively.

From this ROC curve, the optimal cutoff TA size was 5 mm with a sensitivity of 52.6%, specificity of 78.9%, PPV of 51.3%, NPV of 79.8%, and accuracy of 71.1% (p=0.001). There were 5 variables that significantly predicted the diagnosis of the kidney stones when evaluating the TA as shown in Table 3. We proposed a predictive model based on the use of these factors to rate each TA in order to improve the precision of the diagnosis. We found that the use of 5 variables or the use of 4 variables (excluding caliectases because of the extremely low prevalence) did not exhibit significantly different diagnostic values; therefore, we suggested the use of 4 predictive variables to create a predictive model and show how to use the predictive model in some cases in Figure 4.

**Table 3.** *Significant predicting factors.*

| Variable | Beta | Adjusted OR | 95.0% C.I. for OR | p-value | Score |
|---|---|---|---|---|---|
| TA Size (>5 mm) | 1.016 | 2.761 | 1.10-6.92 | 0.030 | 1 |
| Posterior acoustic shadow | 1.586 | 4.884 | 1.06-22.44 | 0.042 | 2 |
| Long tail of TA | 0.935 | 2.548 | 1.01-6.41 | 0.047 | 1 |
| Location at junctional line | 1.032 | 2.806 | 1.12-7.01 | 0.027 | 1 |
| Constant | -2.576 | | | **Total** | **5** |

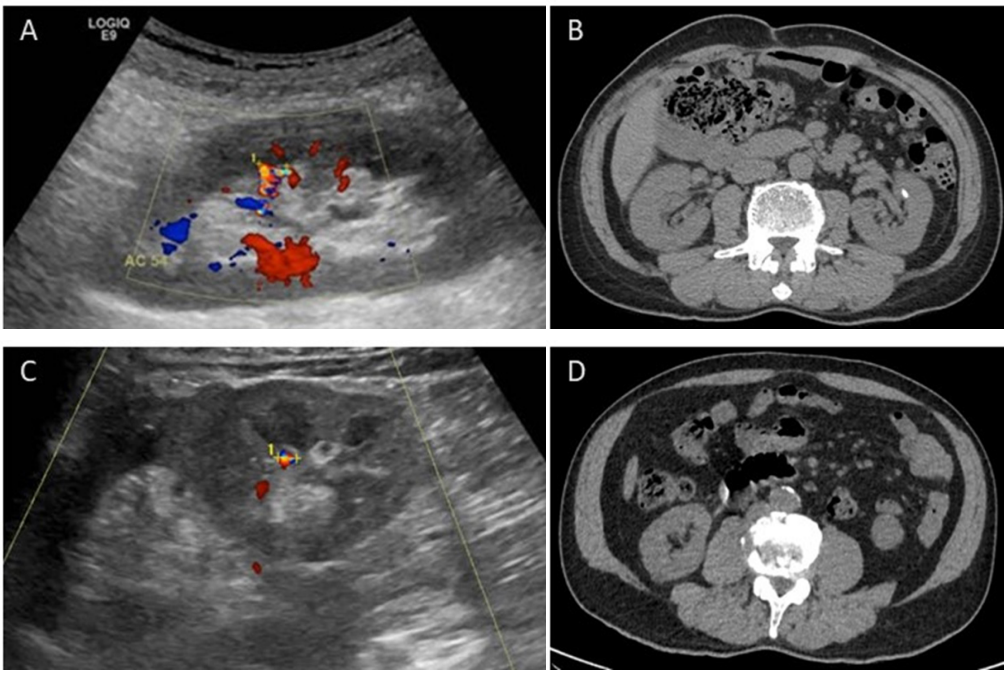


**Figure 4.** *A 51-year-old man with an example of a positive result from the predictive model of nephrolithiasis (A and B). CDUS image (A) shows a TA in the mid pole of the left kidney at the junctional line, with a size of 6.6 mm and a long tail of the TA. The total score of this TA is 3, positive. The unenhanced axial CT image (B) obtained on the same day shows renal stones at the mid pole of the left kidney. In contrast, a 47-year-old woman with an example of a negative result from the predictive model (C and D). The CDUS image(C) shows a TA in the lower pole of the right kidney at the junctional line, with a 4.0 mm size. No demonstrable posterior shadow or long tail of the TA was noted. The total score of this TA is 1, representing a negative result. The unenhanced axial CT image (D) obtained on the same day shows no calculus.*

Then, we additionally collected TAs (53 TAs in total) for model testing. The predicted probabilities for scores=3, 4, and 5 were 60%, 72.7% and 88%, respectively as shown in Table 4. The cutoff scores of 3 or above were positive, with a sensitivity of 75%, specificity of 88%, PPV of 87.5%, NPV of 75.9% (p=0.05) and AUC of 0.82 (95% CI 0.71-0.92). The agreement with the model is 81.13%.

**Table 4.** *Results of testing the predictive model.*

| Score model | Predicted probability |
|---|---|
| 0 | 7.1% |
| 1 | 17.2% |
| 2 | 35.1% |
| 3 | 60.0% |
| 4 | 72.7% |
| 5 | 88.0% |

## Discussion

The TA is a complex phenomenon. Described for the first time in 1996 by Rahmouni et al. [4] , it consists of an intense color signal alternating between red and blue from behind some structures [4]. Two theories have been proposed to explain TAs. The first one was offered by Rahmouni et al. [4], who suggested that this artifact is generated by a strongly reflecting medium with a rough interface. When the incidental beam is reflected on the rough interface, the acoustic wave is split into a complex beam pattern caused by multiple reflections in the medium, resulting in a prolonged pulse duration of the transmitted sound signal; the Doppler units interpret this result as movement and thus assign it different colors. The second theory was offered by Kamaya et al. [13], who stated that the TA is caused by a narrow band of intrinsic sonographic machine noise, referred to as phase or clock jitter, which may be generated by slight random time fluctuations in the path lengths of transmitted and reflected acoustic waves [13].

THE ASEAN JOURNAL OF RADIOLOGY
ISSN 2672-9393

The TA is a diagnostic sign for the reliable evaluation of stones in the urinary tract. Studies [2, 7, 10, 14] have revealed that twinkling artifacts are a useful color Doppler ultrasound tool for the detection of small urinary stones (smaller than 5 mm). However, a high false-positive rate, similar to that in our study, was noted in the study of Dillman et al. [15], with an overall false positive rate of approximately 50%.

A recent meta-analysis study [16] resulted in a pooled sensitivity and specificity in the diagnosis of urolithiasis, with ultrasonographic TA signs of 88.16% [95% confidence interval (CI): 87.07–89.19%] and 79.22% [95% CI: 73.41–84.26%], respectively. There was significant interstudy heterogeneity. The current body of evidence suggests that TAs may be useful as a complementary tool in the diagnostic workup of patients with suspected urolithiasis.

Louvet [17] first found that the TA was dependent on the stone size, with larger stones producing higher artifact grades. Furthermore, Sen et al. [18] reported that when the stone size increased, the sensitivity for the TA in color Doppler US also increased. Our study showed similar results: TA size was significantly related to detected stones in CT, with a moderate ROC area (AUC=0.679, 95% CI 0.579-0.778); the optimal cutoff TA size was 5 mm with a sensitivity of 52.6%, specificity of 78.9%, PPV of 51.3%, NPV of 79.8%, and accuracy of 71.1% (p=0.001).

Simon et al. [19] defined the tail of the TA as “twinkle power”, which supports the theory that microbubbles are present on kidney stones in humans [20, 21]. The stable crevice bubble theory is consistent with previous data that indicate an association between the surface roughness of a stone and the presence of twinkling, as a rougher surface would provide more crevices in which bubbles could form. This is probably a reason why stones usually produce more TA tails (more twinkle power) than other renal calcifications. We found that this associated finding is a positive predictor of kidney stones.

Regarding the location of the TA, the nature of the renal stone location is in the collecting system; thus, a TA located in the renal cortex does not signify a stone. Our study showed that the location in the renal cortex is significantly related to negative CT results. However, there is a TA in the renal cortex, which is a stone in CT due to diffusely increased parenchymal echogenicity with loss of corticomedullary differentiation, in this case, from a chronic kidney disease making it difficult to locate the actual location of this TA.

Our kidney stone predictive model was created to increase accuracy in the diagnosis of kidney stones especially small stones (subcentimeter) in sizes and to improve communication between radiologists and clinicians. The objective checklist includes imaging findings of TAs that are moderately to highly associated with kidney stones. In our study, TA size (≥5 mm), posterior acoustic shadow, long TA tail, junctional line location and Caliectasis each had a statistically significant association with renal stones in CT. The final score has a good confirmational value and expresses the reader's degree of certainty regarding the presence or absence of kidney stones based on the TA. Communication of objective findings in a radiology report serves two purposes. First, radiologists are more accurate when systemically weighing the presence or absence of specific imaging findings before drawing conclusions. Second, a clear list of findings documents the information the radiologist used to determine the final likelihood of renal stones, allowing the referring clinician or surgeon to understand the radiologist's decision-making process. There were limitations to our study. First, our research involved a small number of patients. Second, our study population was restricted to patients who was scheduled  a CT scan from clinical indication of the stone disease which can cause selection bias.  Third, as reported by Aytac and Ozcan [5], the twinkling sign depends on the color sensitivity and the acoustic output of the US unit. Therefore, with different US units, these results might not be reproducible.

THE ASEAN JOURNAL OF RADIOLOGY
ISSN 2672-9393

## Conclusion

In summary, many ultrasound findings with TAs are moderately to highly associated with the presence of kidney stones including the size of TA ≥ 5mm, posterior acoustic shadow, long TA tail, junctional line location and caliectasis. Our TA predictive model for kidney stones moderately improved the accuracy in identifying cases of renal stones with good agreement.

Future studies with larger patient populations will guide the development of the system and will likely provide a sufficiently large dataset for multivariate analysis of kidney stone-specific imaging findings. For now, our data suggest that the likelihood of kidney stones can be more confidently based on the presence of specific imaging findings.

**Competing interests**
The authors declare that they have no competing interests.

**Acknowledgements**
The authors wish to thank the patients who participated in this study.

## References

1. Bultitude M, Rees J. Management of renal colic. BMJ. 2012;345:e5499.

2. Korkmaz M, Aras B, Sanal B, Yucel M, Guneyli S, Kocak A, et al. Investigating the clinical significance of twinkling artifacts in patients with urolithiasis smaller than 5 mm. Jpn J Radiol. 2014;32(8):482-6.

3. Ferrandino MN, Bagrodia A, Pierre SA, Scales CD, Jr., Rampersaud E, Pearle MS, et al. Radiation exposure in the acute and short-term management of urolithiasis at 2 academic centers. J Urol. 2009;181(2):668-72; discussion 73.

4. Rahmouni A, Bargoin R, Herment A, Bargoin N, Vasile N. Color Doppler twinkling artifact in hyperechoic regions. Radiology. 1996;199(1):269-71.

5. Aytac SK, Ozcan H. Effect of color Doppler system on the twinkling sign associated with urinary tract calculi. J Clin Ultrasound. 1999;27(8):433-9.

6. Lee JY, Kim SH, Cho JY, Han D. Color and power Doppler twinkling artifacts from urinary stones: clinical observations and phantom studies. AJR Am J Roentgenol. 2001;176(6):1441-5.

7. Hanafi MQ, Fakhrizadeh A, Jaafaezadeh E. An investigation into the clinical accuracy of twinkling artifacts in patients with urolithiasis smaller than 5 mm in comparison with computed tomography scanning. J Family Med Prim Care. 2019;8(2):401-6.

8. Masch WR, Cohan RH, Ellis JH, Dillman JR, Rubin JM, Davenport MS. Clinical Effectiveness of Prospectively Reported Sonographic Twinkling Artifact for the Diagnosis of Renal Calculus in Patients Without Known Urolithiasis. AJR Am J Roentgenol. 2016;206(2):326-31.

THE ASEAN JOURNAL OF RADIOLOGY
ISSN 2672-9393

9. Winkel RR, Kalhauge A, Fredfeldt KE. The usefulness of ultrasound colour-Doppler twinkling artefact for detecting urolithiasis compared with low dose nonenhanced computerized tomography. Ultrasound Med Biol. 2012;38(7):1180-7.

10. Yavuz A, Ceken K, Alimoglu E, Kabaalioglu A. The reliability of color doppler "twinkling" artifact for diagnosing millimetrical nephrolithiasis: comparison with B-Mode US and CT scanning results. J Med Ultrason (2001). 2015;42(2):215-22.

11. Masch WR, Cronin KC, Sahani DV, Kambadakone A. Imaging in Urolithiasis. Radiol Clin North Am. 2017;55(2):209-24.

12. Kielar AZ, Shabana W, Vakili M, Rubin J. Prospective evaluation of Doppler sonography to detect the twinkling artifact versus unenhanced computed tomography for identifying urinary tract calculi. J Ultrasound Med. 2012;31(10):1619-25.

13. Kamaya A, Tuthill T, Rubin JM. Twinkling artifact on color Doppler sonography: dependence on machine parameters and underlying cause. AJR Am J Roentgenol. 2003;180(1):215-22.

14. Bacha R, Manzoor I, Gilani SA, Khan AI. Clinical Significance of Twinkling Artifact in the Diagnosis of Urinary Stones. Ultrasound Med Biol. 2019;45(12):3199-206.

15. Dillman JR, Kappil M, Weadock WJ, Rubin JM, Platt JF, DiPietro MA, et al. Sonographic twinkling artifact for renal calculus detection: correlation with CT. Radiology. 2011;259(3):911-6.

16. Laher AE, McDowall J, Gerber L, Aigbodion SJ, Enyuma COA, Buchanan S, et al. The ultrasound 'twinkling artefact' in the diagnosis of urolithiasis: hocus or valuable point-of-care-ultrasound? A systematic review and meta-analysis. Eur J Emerg Med. 2019;27(1):13-20.

17. Louvet A. Twinkling artifact in small animal color-Doppler sonography. Vet Radiol Ultrasound. 2006;47(4):384-90.

18. Sen V, Imamoglu C, Kucukturkmen I, Degirmenci T, Bozkurt IH, Yonguc T, et al. Can Doppler ultrasonography twinkling artifact be used as an alternative imaging modality to non-contrast-enhanced computed tomography in patients with ureteral stones? A prospective clinical study. Urolithiasis. 2017;45(2): 215-9.

19. Simon JC, Holm JR, Thiel J, Dunmire B, Cunitz BW, Bailey MR. Evidence of microbubbles on kidney stones in humans. Ultrasound Med Biol. 2020;46(7):1802-7.

20. Kim HC, Yang DM, Jin W, Ryu JK, Shin HC. Color Doppler twinkling artifacts in various conditions during abdominal and pelvic sonography. J Ultrasound Med. 2010;29(4):621-32.

21. Lu W, Sapozhnikov OA, Bailey MR, Kaczkowski PJ, Crum LA. Evidence for trapped surface bubbles as the cause for the twinkling artifact in ultrasound imaging. Ultrasound Med Biol. 2013;39(6):1026-38.

THE ASEAN JOURNAL OF RADIOLOGY
ISSN 2672-9393

Original Article

# Randomised trial on pain reduction in hysterosalpingography - a modified technique without vulsellum forceps

*Olubukola AT Omidiji, F.M.C.R., M.P.H.*[(1)]
*Omodele A Olowoyeye, F.M.C.R. Ph.D.*[(1)]
*Richard Efidi, F.M.C.R.*[(2)]
*Omololu Adegbola, F.M.C.O.G.*[(3)]
*Oluyemisi O.Toyobo, F.M.C.R.*[(2)]
*Ogonna Okeke, M.B.B.S.*[(1)]
*Thaddeus N Opara, F.M.C.R.*[(4)]
*Abidemi Shabi, M.B.B.S.*[(4)]
From Departments of [(1)]Radiation Biology, Radiotherapy, Radiodiagnosis and Radiography and [(3)]Obstetrics and Gynaecology, College of Medicine, University of Lagos/ Lagos University Teaching Hospital, Idi-Araba,
[(2)]Crestview Radiology,
[(4)]Department of Radiology, Federal Medical Centre, Ebute Metta, Lagos, Nigeria.
Address correspondence to Omidiji O.A.(tomidiji@unilag.edu.ng)

Received 21 September 2022 ; revised 1 December 2022 ; accepted 15 December 2022
doi:10.46475/aseanjr.v23i3.187

## Abstract

**Background:** Pain is the most common side effect of hysterosalpingography (HSG) and partly arises from vulsellum placement on the cervix and cervical traction.

**Objective:** To study the effect of conducting HSG without grasping the cervix with vulsellum forceps on the time taken to complete the procedure, pain experienced by the participants and diagnostic quality of HSG images produced.

**Materials and Methods:** A randomized controlled trial of 64 consenting adult women referred to the Radiodiagnostic department for HSG from July to December 2020 was carried out. The women were consecutively selected and randomly distributed into two groups: Group 1 - no cervical grasp and Group 2 – with cervical grasp with vulsellum forceps. HSG was done using a fluoroscopy machine, following the standard hospital protocol with speculum, Leech Wilkinson cannula and Urografin 76%. Procedure time, procedure pain using the visual analog scale and diagnostic quality of images were assessed. Data analysis was done using Microsoft Excel and SPSS software version 22.

**Results:** The overall mean duration of the procedure was 12.59 minutes. There was no significant difference in the procedure duration between both groups. The overall mean pain scores immediately and 15 minutes after the procedure were 4.83 and 2.23 respectively. Significant differences in pain scores were seen in the immediate post procedure 3.94 (group 1) versus 5.72 (group 2) and 15 minutes post procedure 1.75 (group 1) versus 2.72 (group 2). After adjusting for confounders, the pain score was noted to be significantly related to the HSG technique with vulsellum use associated with the higher immediate post HSG pain score. No significant difference was seen in the diagnostic image quality between group I and II.

**Conclusion:** The elimination of vulsellum forceps during hysterosalpingography was associated with reduced pain in the immediate and 15 minutes after the procedure, without significantly increasing the procedure duration. It had no deleterious effect on the image quality.

**Keywords:** HSG, Technique, Pain, Cervical grasp, Vulsellum, Procedure duration.

THE ASEAN JOURNAL OF RADIOLOGY
ISSN 2672-9393

## Introduction

Hysterosalpingography (HSG) is a radiologic modality used in investigating female factor infertility [1]. It involves the instillation of contrast or dye through the cervix to outline the uterine cavity and establish tubal patency [1]. It is often associated with pain, in some cases warranting sedation and pain medication.

Pain is the most common side effect of HSG and arises from tenaculum placement on the cervix, cervical traction, instillation of dye through a cannula and tubal spillage of dye [2]. A study by Atalabi et al on x-ray hysterosalpingography showed that cervical traction with the introduction of cannula was the most painful part of the procedure with median pain of 6 on a 0-10 visual acuity scale [3].

Grasping of the cervix using a tenaculum/vulsellum forceps is usually done for adequate stabilization of the cannula [3]; however, this can result in more pain and distress and a negative experience if not placed adequately. Some studies have shown that gentle slow placement reduces the pain, but does not eliminate the pain completely [4,5]. These studies were conducted for intrauterine device insertion. Variations for grasping the cervix have not been considered for HSG.

A study by Unlu et al on comparison of four different pain relief methods during hysterosalpingography was able to eliminate pain from tenaculum placement using oral naproxen tablets, injections and topical creams [6]. These drugs are not without their own side effects.

The aim of the study was to ascertain whether conducting HSG without grasping the cervix with vulsellum forceps was feasible and to document the effect on time taken to complete the procedure, pain experienced by the participants and morphology of HSG images *vis* a *vis* the outlined uterine cavities and tubes.

## Materials and methods

This was a prospective study and a randomized controlled trial of consenting adult women who were referred to the hospital for HSG on account of infertility. Approval for the study was obtained from the Health Research Ethics Committee of Lagos University Teaching Hospital (ADM/DCST/HREC/APP/2511). All patients who presented at the center between 15 July and 14 December 2020 were included into the study. Sixty four (64) consecutive women who were referred for the procedure were randomly distributed into 2 groups, namely group 1 no cervical grasp and group 2 with cervical grasp.

Odd numbers were pre-assigned as group 1 and even numbers were pre-assigned as group 2. Each participant was asked to pick an envelope containing a number. The envelope is opened by the patient and the number was handed over to the radiologist.

Informed oral and written consent was obtained from the participants prior to the commencement of the study. A proforma to obtain sociodemographic, clinical and gynaecological history was administered to the patient. Women with known stenotic cervical os, acute cervicitis, intense anxiety, a history of any allergy to radio-opaque dye, any recent history of acute pelvic inflammatory disease, any abnormal vaginal discharge (known to exacerbate and flare up following HSG), any other cause of chronic pelvic pain, a positive β-human chorionic gonadotropin test, or were <18 years of age and participants with patulous cervix were excluded from the study.

Sample size determination was done using the formula for equivalence design of randomized control trial as detailed below [7]:

THE ASEAN JOURNAL OF RADIOLOGY
ISSN 2672-9393

Prevalence of women with moderate to severe pain during tenaculum placement: 78.7% p = 0.79 [3].

Minimum acceptable margin $\delta_0 = 0.21$

$$N = 2 \times \left( \frac{z_{1-\frac{\alpha}{2}} + z_{1-\beta}}{\delta_0} \right)^2 \times p \times (1-p)$$

$$N = 2 \, x \left[ \frac{1.96 + 0.68}{0.19} \right] x \, 0.79 \, x \, 0.21 \; = 52.7.$$

*Twenty percent (20%) attrition was added, giving a total of 64 participants*

**Technique of Hysterosalpingography at the centre**

A fluoroscopy machine Apelem VBS and a bucky table were used in the procedure. Participants were booked during the proliferative phase (day 8 – 12) of the menstrual cycle, when the endometrium was thinnest.[1] They were advised to abstain from sexual intercourse from the start of their period till after the procedure.

On the day of the procedure, an intravenous line was secured prior to the procedure, for the purpose of resuscitation in case of contrast reaction. Hospital gowns were provided to the patients to wear after removing their clothes and underwear.

Scout films (antero-posterior [AP] of the pelvis) were obtained to ascertain good radiographic factor settings and also to detect any premorbid condition.

The patients were placed in the lithotomy position, with the thighs flexed and abducted, the feet resting in stirrups, and the buttocks extending slightly beyond the edge of the examining table for the ease of examination.

The perineum and vagina were cleaned with an antiseptic using a sponge holding forceps and sterile gauze. The vagina and perineal area were cleansed before speculum insertion.

The patients' external genitalia were inspected. Under an aseptic condition and bright illumination, the labia were parted and a disposable plastic Cusco's speculum lubricated with xylocaine gel was inserted into the vagina with the blades held obliquely and pressure exerted toward the posterior vaginal wall to avoid the more sensitive anterior wall and urethra. The blades were rotated into a horizontal position, and opened after full insertion, then maneuvered so that the cervix came into full view. The speculum was secured with the blades open by tightening the thumbscrew.

For group 1, the vulsellum forceps were not utilized. For group 2, the anterior lip of the cervix was grasped with a vulsellum forceps. Participants were blinded to the group they fell in.

An appropriate size Leech Wilkinson's cannula was selected and inserted into the distal end of the cervical canal, after prefilling with contrast medium to eliminate air bubbles. While maintaining a tight seal between the cervical canal and the cannula, a water-soluble contrast medium, Urografin 76% (20 mL contains sodium amidotrizoate 200 g and meglumineamidotrizoate 1320 g, with iodine concentration of 370 mg/mL, diluted with water for injection in ratio 1:1, to prevent peritoneal irritation) was instilled slowly into the uterine cavity and the fallopian tubes under fluoroscopic guidance. About 7-20 mL of contrast medium was instilled with higher volume in grossly dilated uterine cavities. The contrast medium was instilled in a slow and steady fashion while watching its progress under fluoroscopy.

Before film exposure, the position of the marker was ascertained. Early radiograph of the uterine cavity when it first fills with contrast medium was obtained because further instillation of contrast medium can sometimes obscure intracavitary pathology. Continuous contrast medium instillation and intermittent fluoroscopy

THE ASEAN JOURNAL OF RADIOLOGY
ISSN 2672-9393

screening was done, and the film exposed when the tubes filled and spilled into the peritoneal cavity. Patients were turned to right or left oblique position to delineate the fallopian tubes better if necessary.

Pelvic radiographs were obtained in AP supine and right and left oblique positions during the instillation of the contrast medium. Delayed radiographs were obtained 30 minutes after completion of the procedure, as necessary, to assess the degree of loculation of contrast medium in the peritoneal cavity.

**Measure**s

A. Procedure duration in each patient was determined.
Timing commenced after insertion of speculum and ended just before the removal of the speculum.

B. Procedure pain.
In both groups, the pain of the procedure was scored immediately after and 15 minutes after the HSG completed and instruments were removed.
Patients were asked to rate their pain during HSG using a 0 to 10 visual analogue scale (VAS), (0 = no pain, 10 = worst possible pain). VAS scores were measured and recorded in real time by the same radiologist.

C. Diagnostic quality of images:

1. Poor (uterine cavity, tubes and cervical canal not clearly depicted)
2. Average (uterine cavity and tubes clearly depicted, excluding the cervical canal)
3. Good (uterine cavity, cervical canal and tubes clearly depicted)

**Image analysis**

One radiologist performed all the procedures while the films were reviewed by performing radiologist with two other experienced radiologists reviewing the HSG images with consensus.

### Data analysis

The data was entered using Microsoft Excel and analyzed using the SPSS software, Chicago, IL, USA for Windows version 22 program. Chi-square test was used for comparison between categorical variables and Student T-test for comparison between continuous variables in both groups. The different pain scores were tested for normality by Shapiro-Wilk test. A multivariate stepwise linear regression model was conducted to assess if the use of vulsellum forceps was associated with increased pain. A P value <0.05 was regarded as a significant value.

## Results

### Demographic and clinical characteristics

A total of 64 consenting women who presented for hysterosalpingography procedure at the radiology department/diagnostic centre were included in the study, randomized into two groups; group 1 without cervical grasp (32 women) and group 2 (32 women) with cervical grasp (Table 1).

The mean ages were 35.63 years and 35.94 years for groups 1 and 2 respectively with no significant difference in age between the comparison groups (p-value > 0.05).

The overall mean duration of the procedure was 12.59 minutes. Group I had a higher mean of 13.2 minutes, which was, however, not statistically significant.

The mean pain scores immediately and 15 minutes after the procedure were also lower in group 1(3.94; 1.75) compared with group 2 (5.72, 2.72).

The overall mean pain reduction score was also lower in group 1 than in group 2 (2.19 versus 2.59). This was, however, not statistically significant.

THE ASEAN JOURNAL OF RADIOLOGY
ISSN 2672-9393

**Table 1.** *Demographic and clinical characteristics of the study population.*

| Clinical characteristics | No vulsellum | | | Vulsellum | | | Total | | | p-value |
|---|---|---|---|---|---|---|---|---|---|---|
| | N | Range | Mean ± SD | N | Range | Mean ± SD | N | Range | Mean ± SD | |
| Age(years) | 32 | 28-43 | 35.63 ± 3.97 | 32 | 28-43 | 35.94 ± 3.37 | 64 | 28-43 | 35.78 ± 3.66 | 0.736 |
| Number of days post-menses | 31* | 8-12 | 10.35 ± 1.11 | 31* | 9-12 | 10.71 ± 0.86 | 62 | 8-12 | 10.53 ± 1.00 | 0.115 |
| Parity | 32 | 0-4 | 1.00 ± 1.16 | 32 | 0-4 | 1.22 ± 1.26 | 64 | 0-4 | 1.11 ± 1.21 | 0.934 |
| Duration of HSG(minutes) | 32 | 5-45 | 13.22 ± 7.53 | 32 | 5-20 | 11.97 ± 3.33 | 64 | 5-45 | 12.59 ± 5.81 | 0.394 |
| Pain score immediate post-HSG | 32 | 0-8 | 3.94 ± 1.98 | 32 | 4-9 | 5.72 ± 1.37 | 64 | 0-9 | 4.83 ± 1.92 | <0.001 |
| Pain score 15minutes post-HSG | 32 | 0-8 | 1.75 ± 1.81 | 32 | 1-8 | 2.72 ± 1.80 | 64 | 0-8 | 2.23 ± 1.86 | 0.036 |
| Pain score reduction from 0 – 15 minutes | 32 | -3-7 | 2.19 ± 2.05 | 32 | -2-7 | 3.00 ± 1.85 | 64 | -3 -7 | 2.59 ± 1.98 | 0.101 |

**Two women had amenorrhoea, one in each group*

Thirty (30; 46.8%) participants were sent on account of primary infertility and twenty-nine (29, 45.3%) on account of secondary infertility. Twenty-eight (28; 43.8%) patients had a history of previous HSG and only 4(6.3%) had done sonohysterosalpingography (Table 2).

**Table 2.** *Clinical characteristics of participants in each group.*

| Clinical characteristics | | Group 1: No vulsellum (n = 32) Frequency (% of total) | Group 2: Vulsellum (n = 32) Frequency (% of total) | p-value |
|---|---|---|---|---|
| **Indication** | Primary infertility | 15 (23.4) | 15 (23.4) | 0.346 |
| | Secondary Infertility | 13 (20.3) | 16 (25) | |
| | Amenorrhoea | 1 (1.6) | 1 (1.6) | |
| | Uterine Fibroids | 3 (4.7) | 0 (0) | |
| History of previous pregnancy | No | 16 (25) | 14 (21.9) | 0.616 |
| | Yes | 16 (25) | 18 (28.1) | |
| History of miscarriage/ abortion | No | 17 (26.6) | 16 (25) | 0.802 |
| | Yes | 15 (23.4) | 16 (25) | |
| Past history of Pelvic Inflammatory Disease | No | 15 (23.4) | 15 (23.4) | 1.000 |
| | Yes | 17 (26.6) | 17 (26.6) | |
| History of Lower Abdominal Pain | No | 22 (34.4) | 24 (37.5) | 0.578 |
| | Yes | 10 (15.6) | 8 (12.5) | |
| History of Lower Abdominal Pain | No | 10(15.6) | 15 (23.4) | 0.200 |
| | Yes | 22 (34.4) | 17 (26.6) | |
| Previous Pelvic USS study | No | 3 (4.7) | 4 (6.2) | 0.689 |
| | Yes | 29 (45.3) | 28 (43.8) | |
| Previous Sono-HSG Study | No | 31 (48.4) | 29 (45.3) | 0.302 |
| | Yes | 1 (1.6) | 3 (4.7) | |
| Previous HSG Study | No | 20 (31.2) | 16 (25) | 0.313 |
| | Yes | 12 (18.8) | 16 (25) | |
| History of Previous Surgery | No | 25 (39.1) | 23 (35.9) | 0.564 |
| | Yes | 7 (10.9) | 9 (14.1) | |

THE ASEAN JOURNAL OF RADIOLOGY
ISSN 2672-9393

**Association between technique of HSG and pain score immediately after and 15 minutes after procedure**

In view of the non-normality of the distribution of pain score immediately after the procedure, with respect to the HSG technique (p<0.001; Shapiro-Wilk test), the independent-samples Mann-Whitney U non-parametric test was employed, which demonstrated a significant association (p< 0.001) between the pain score immediately after procedure and the technique of HSG. The performance of HSG without vulsellum is associated with a reduced pain score immediately after the procedure. There was also significant association between the technique of HSG and the pain score 15 minutes after the procedure (P= 0.007) (Table 3).

**Table 3.** *Association between technique of HSG and pain score immediately after and 15 minutes after procedure.*

| | | Pain score immediately after HSG | | |
|---|---|---|---|---|
| **Technique of HSG** | **n** | **Mean rank** | **Standardised test statistic** | **p-value** |
| No vulsellum | 32 | 23.56 | 3.936 | <0.001 |
| Vulsellum | 32 | 41.44 | | |
| | | **Pain score 15 minutes after HSG** | | |
| **Technique of HSG** | **n** | **Mean rank** | **Standardised test statistic** | **p-value** |
| No vulsellum | 32 | 26.41 | 2.699 | 0.007 |
| Vulsellum | 32 | 38.59 | | |

**Association between the technique of HSG and reduction in the pain score from 0 – 15 minutes after HSG**

Using the non-parametric Mann-Whitney U test because of the non-normality in the distribution of the reduction in pain score from 0 – 15 minutes after HSG (Shapiro-Wilk test), there is no significant association (p = 0.907) between the technique of HSG and the pain score reduction (Table 4).

**Table 4.** *Association between technique of HSG and reduction in pain score from 0 – 15 minutes after HSG.*

| | Pain score reduction from 0 to 15 minutes after HSG | | | |
|---|---|---|---|---|
| **Technique of HSG** | **n** | **Mean rank** | **Standardised test statistic** | **p-value** |
| No vulsellum | 32 | 28.69 | 1.671 | 0.095 |
| Vulsellum | 32 | 36.31 | | |

**Association between technique of HSG and procedure duration**

Using the non-parametric Mann-Whitney U test because of the non-normal distribution of the procedure duration (p<0.001; Shapiro-Wilk test), we found no significant association (P= 0.907) between the technique of HSG and the procedure duration (Table 5).

**Table 5.** *Association between technique of HSG and procedure duration.*

| | Procedure duration | | | |
|---|---|---|---|---|
| **Technique of HSG** | **n** | **Mean rank** | **Standardised test statistic** | **p-value** |
| No vulsellum | 32 | 32.23 | 0.117 | 0.907 |
| Vulsellum | 32 | 32.77 | | |

THE ASEAN JOURNAL OF RADIOLOGY
ISSN 2672-9393

**Relationship between the pain score immediately after the procedure and demographic/clinical characteristics/HSG technique**

Multiple linear regression was performed to model the relationship between pain score immediately after the procedure and demographic/clinical characteristics/HSG technique, while adjusting for the presence of confounders. The result showed that the pain score immediately after the procedure, adjusted for other possible confounders, is significantly related to HSG technique; the use of vulsellum is associated with a higher immediate post-HSG pain score. The other parameters do not, however, show a significant relationship with the immediate post-HSG pain score (Table 6).

**Table 6.** *Relationship between pain score immediately after procedure and demographic/clinical characteristics/HSG technique.*

| Model | Standardized Coefficients | t | p-value | 95.0% Confidence Interval | |
|---|---|---|---|---|---|
| | Beta | | | Lower Bound | Upper Bound |
| (Constant) | | -0.362 | 0.719 | -6.214 | 4.316 |
| Age | 0.143 | 1.057 | 0.295 | -0.067 | 0.217 |
| Duration of HSG | 0.035 | 0.246 | 0.807 | -0.082 | 0.105 |
| Technique of HSG | 0.463 | 3.911 | <0.001 | 0.857 | 2.665 |
| Ever pregnant | -0.065 | -0.211 | 0.834 | -2.588 | 2.096 |
| History of abortion | -0.101 | -0.309 | 0.759 | -2.871 | 2.105 |
| Past history of PID | -0.077 | -0.542 | 0.590 | -1.381 | 0.794 |
| Any lower abdominal pain | -0.138 | -0.921 | 0.361 | -1.850 | 0.686 |
| Any history of fibroid | -0.010 | -0.081 | 0.936 | -1.034 | 0.954 |
| Any previous HSG | 0.122 | 0.895 | 0.375 | -0.581 | 1.516 |
| Any pelvic surgery | 0.020 | 0.151 | 0.881 | -1.087 | 1.264 |
| Reason for test | 0.144 | 0.838 | 0.406 | -0.505 | 1.228 |

**The relationship between the pain score 15 minutes after the procedure and the demographic/clinical characteristics/HSG technique**

Multiple linear regression was again performed to model the relationship between the 15-minute post-procedure pain score and the demographic/clinical characteristics/HSG technique, while adjusting for the presence of confounders. The result showed that the 15-minute post-procedure pain score, adjusted for other possible cofounders, is significantly related to the HSG technique, and the past history of pelvic inflammatory disease (PID). Hence, the use of vulsellum is associated with higher 15-minute post-procedure pain score. Similarly, the past history of PID was associated with the higher 15-minute post-procedure pain score. The other parameters do not, however, show a significant relationship with the 15-minute post-HSG pain score (Table 7).

**Table 7.** *Relationship between pain score 15 minutes after procedure and demographic/clinical characteristics/HSG technique.*

| Model | Standardized Coefficients | t | p-value | 95.0% Confidence Interval | |
|---|---|---|---|---|---|
| | Beta | | | Lower Bound | Upper Bound |
| (Constant) | | 0.579 | 0.565 | -3.528 | 6.389 |
| Age | -0.087 | -0.666 | 0.509 | -0.178 | 0.090 |
| Duration of HSG | 0.067 | 0.492 | 0.625 | -0.066 | 0.109 |
| Technique of HSG | 0.235 | 2.047 | 0.046 | 0.017 | 1.719 |
| Ever pregnant | -0.088 | -0.296 | 0.769 | -2.531 | 1.881 |
| History of abortion | -0.339 | -1.073 | 0.288 | -3.595 | 1.091 |
| Past history of PID | 0.301 | 2.176 | 0.034 | 0.086 | 2.134 |
| Any lower abdominal pain | -0.154 | -1.059 | 0.295 | -1.824 | 0.565 |
| Any history of fibroid | -0.247 | -2.000 | 0.051 | -1.869 | 0.003 |
| Any previous HSG | 0.258 | 1.947 | 0.057 | -0.030 | 1.945 |
| Any pelvic surgery | 0.046 | 0.352 | 0.726 | -0.913 | 1.302 |
| Reason for test | 0.253 | 1.523 | 0.134 | -0.197 | 1.435 |

THE ASEAN JOURNAL OF RADIOLOGY
ISSN 2672-9393

**Diagnostic quality of images**

Diagnostic quality of images was good in both the vulsellum and non-vulsellum groups while no case was poor in either group. Hence, there is no significant difference (P = 1.000) in the diagnostic image quality between the vulsellum and no-vulsellum groups (Table 8, Figures 1,2).

**Table 8.** *Association between technique of HSG and diagnostic quality of the images.*

| Technique of HSG | Diagnostic quality of the images | | | Total | p-value |
|---|---|---|---|---|---|
| | Poor | Average | Good | | |
| No vulsellum | 0 | 2 | 30 | 32 | |
| Vulsellum | 0 | 1 | 31 | 32 | 1.000 |
| Total | 0 | 3 | 61 | 64 | |

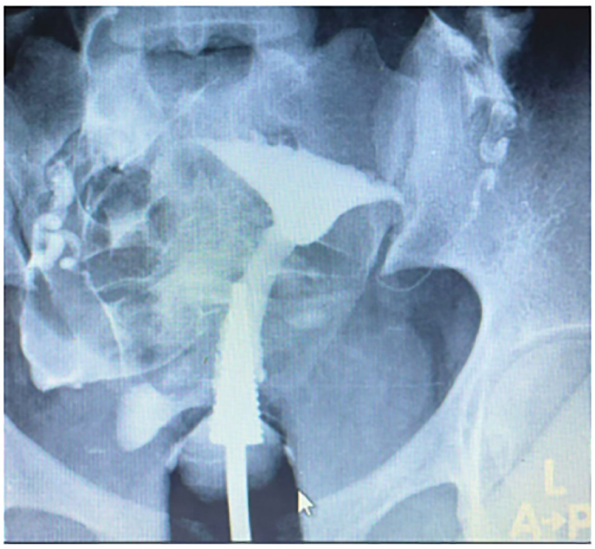


**Figure 1.** *HSG image without vulsellum: This demonstrates the uterine cavity and tubes with bilateral free peritoneal contrast spillage. Diagnostic image quality was 3 -good.*

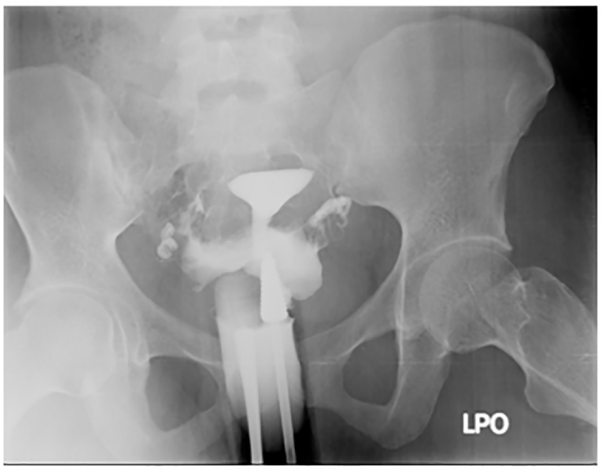


**Figure 2.** *HSG image with vulsellum shows the uterine cavity and tubes with bilateral free peritoneal contrast spillage. Diagnostic image quality was 3 - good.*

## Discussion

Several studies have been done to assess ways of pain alleviation during hysterosalpingography. Pain is experienced at various stages in the procedure; The main factors producing pain are cervical traction and fast instillation of contrast into the uterine cavity causing uterine contraction [3]; hence, slow instillation of the dye is recommended to obviate this. An individual radiologist is also one of the factors associated with pain during and after HSG. This study aimed to assess the possibility of pain reduction through the elimination of usage of vulsellum during the procedure.

The mean age of participants who presented for the hysterosalpingography procedure in this study on account of infertility is similar to those of other studies [8,9,10]. Mean ages in recent studies range from 32-36 years.

The majority of the participants (92%) had infertility as indication for hysterosalpingography. Less than half (45%) were on account of secondary infertility. This did not correlate with that of the study by Onwuchekwa et al, in which they documented that 81.6% of their 250 study participants was on account of secondary infertility [8]. Toufig et al noted that the indication depended on the

THE ASEAN JOURNAL OF RADIOLOGY
ISSN 2672-9393

age group being researched. They noted that in the 15-25 year age group, the sole indication was primary infertility, while in the 26-45 year age group, secondary infertility dominated [11]. The difference noted may be due to the smaller sample size in this study.

About 43-48% of the participants had a previous history of hysterosalpingography and abortions/miscarriages, the percentage is higher than seen in Toufig et al likely because they only recorded those who had complications such as infections or pathologies such as blocked tubes in their history taking [12].

Sonohysterosalpingography, also called hysterosonography is the technique implemented under ultrasound guidance which involves the introduction of a catheter into the endometrial cavity and instillation of sterile saline to outline the uterine cavity. This provides detail of the endometrial lining. It is a procedure often done prior to assisted conception [12]. Only 6.3% of the participants had done sonohysterosalpingography, which suggests preference for HSG over the former, most likely because of the limitation of sonohysterosalpingography in assessing the tubes [13].

The procedure duration of HSG varies per location or institution. [13] It has been recorded as taking 10 to 45 minutes [14-16], which includes the time for the patient to lie on the couch and take the first film till the patient is off the couch. Another study that discussed timing during HSG only discussed the intervals between the first HSG image and distal tubal filling, and interval between distal tubal filling and the last HSG image. The intervals ranged from 8.4 secs to 80 secs [17]. The procedure duration in this study ranged from 12 to 21 minutes, excluding the time for patient preparation.

There was no significant difference in duration in the non-vulsellum group, compared with the vulsellum group. To our knowledge, no study has shown the time between post speculum insertion and pre speculum removal, neither have they shown timing of vulsellum placement.

Many side effects of HSG have been described such as nausea, vomiting, infection, bleeding and pain. Pain is the most common side effect of HSG and one which causes fear and anxiety among women, with a negative impact on patient cooperation [18]. According to Unlu et al, most of the women found the procedure acutely painful at the point of placement of the tenaculum, cervical traction, dye instillation and tubal spillage [7]. Grasping the cervix with a tenaculum or vulsellum may release prostaglandins which can initiate uterine cramps resulting in pain [19]. Liberty et al also stated in their study that cervical instrument insertion was the most painful step of the procedure [20]. This was also noted in this study as using the visual analog scale, vulsellum placement was associated with a higher immediate post-HSG pain score, compared with non-vulsellum placement. A similar finding was described by Atalabi et al [3]. It was discovered in Unlu et al's study on comparison of four different pain relief methods during HSG that local application of lidocaine cream in addition to 500mg NSAID nonsteroidal anti-inflammatory drug (Naproxen®) helped to reduce the pain [7]. Yet, another study hypothesized the use of non-opioid analgesia as the most preferred prophylactic method; however, a Cochrane review reported that beneficial effect of the analgesia could not be ascertained, compared with the placebo up to 30 minutes after the procedure [21]. Intracervical and paracervical blocks have also been researched by some, this enabled patients to tolerate pain during tenaculum placement and subsequent traction [9,19,22]. These blocks are done by submucosal injection of 2% lidocaine at 12'0'clock, 4'o'clock and 8'o'clock positions, lateral and posterior to the uterocervical junctions. This is not without side effects of injecting the wrong sites and having lidocaine in the blood stream [19,22].

Other ways of eliminating pain involve the use of balloon catheters [23]. Balloon catheters have been seen to cause less pain compared with metal cannulas; however, this does not eliminate the pain from tenaculum placement [24]. We believe for some patients, even with balloon catheters, tenaculum or vulsellum placement can be completely eliminated.

THE ASEAN JOURNAL OF RADIOLOGY
ISSN 2672-9393

The overall mean score for 15 minutes post procedure pain was reduced compared with the immediate post procedure. Also noted is a reduction in the pain score for those in the non-vulsellum group compared with the vulsellum group. According to Ayida et al, pain perception gradually decreases, ending 30 minutes after the procedure in a high percentage of patients with mild to moderate pain during the procedure [25].

Other techniques have also eliminated the use of vulsellum or tenaculum [26]. One of such is the use of a cervical vacuum cup. The cup stays on the cervix through a vacuum and contrast is then instilled into the uterine cavity. While this eliminates the pain from tenaculum placement, when compared with the balloon catheter, the procedure was harder to perform and took longer time. The balloon catheter was also better tolerated.

For patients with patulous cervix, larger catheters or 8F paediatric Foley catheters can be utilized instead of the 5F catheters [27].

The type of procedure did not affect the image quality. Both the vulsellum and non-vulsellum groups gave good quality images.

**Limitation:**
The study was institution-based.

## Conclusion

The elimination of vulsellum forceps during hysterosalpingography was associated with reduced pain in the immediate and 15 minutes after the procedure, without significantly increasing the procedure duration. It had no deleterious effect on the image quality.

Multicentre studies are advised to confirm our findings with a larger sample size.

## References

1. Lawan RO, Ibinaiye PO, Onwuafua P, Hamidu A. Evaluation of Pattern of Tubo-peritoneal Abnormalities Potentially Responsible for Infertility in Zaria, Nigeria: Hysterosalpingographic Assessment. Sub-Saharan Afr J Med 2015;2:110 – 6. doi:10.4103/2384-5147.164418.

2. Robinson RD, Casablanca Y, Pagano KE, Arthur NA, Bates GW, Propst AM. Intracervical block and pain perception during the performance of a hysterosalpingogram: a randomized controlled trial. Obstet Gynecol 2007;109:89-93. doi: 10.1097/01.AOG.0000247645.52211.41.

3. Atalabi OM, Osinaike BB. X-ray Hysterosalpingography: the most painful part in the Nigerian woman. Afr J Anaesth Intensive Care 2011;11:24-8. doi:10.4314/ajaic.v11i1.69133.

4. Medcape [Internet]. New York: WebMD; c1994-2022 [updated 2021 Sep 21; cited 2022 Nov 16]. Hysterosalpingogram Technique. Available from: https://emedicine.medscape.com/article/2111999-technique#c1.

5. Abbas AM, Abdelkadera AM, Elsayed AH, Fahmy MS. The effect of slow versus fast application of vulsellum on pain perception during copper intrauterine device insertion: a randomized controlled trial. Middle East Fertil Soc J 2018;23:143–7.

6. Unlu BS, Yilmazer M, Koken G, Arioz DT, Unlu E, Baki ED, et al.Comparison of four different pain relief methods during hysterosalpingography: a randomized controlled study. Pain Res Manag 2015;20:107-1. doi: 10.1155/2015/306248.

7. Zhong B. How to calculate sample size in randomized controlled trial? J Thorac Dis 2009;1:51-4.

8. Onwuchekwa CR, Oriji VK. Hysterosalpingographic (HSG) pattern of infertility in women of reproductive age. J Hum Reprod Sci 2017;10:178-84. doi:10.4103/jhrs.JHRS_121_16.

9. Eduwem DU, Akintomide AO, Bassey DE, Ekott MI. Hysterosalpingographic patterns and relevance in the management of infertility in a Nigerian tertiary health Institution. Asian J Med Sci 2016;7:70-4.

10. Omidiji OA, Toyobo OO, Adegbola O, Fatade A, Olowoyeye OA. Hysterosalpingographic findings in infertility – what has changed over the years? Afr Health Sci2019;19:1866-74. doi: 10.4314/ahs.v19i2.9.

11. Toufig H, Benameur T, Twfieg ME, Omer H, El-Musharaf T. Evaluation of hysterosalpingographic findings among patients presenting with infertility. Saudi J Biol Sci 2020;27:2876-82. doi: 10.1016/j.sjbs.2020.08.041.

12. Obajimi G, Ogunkinle B. Routine saline infusion sonohysterography prior to assisted conception: a review of our initial experience. Ann Ib Postgrad Med 2016;14:99-102.

13. Allison SJ, Horrow MM, Kim HY, Lev-Toaff AS. Saline-infused Sonohysterography: Tips for achieving greater success. Radiographics 2011;31:1991-2004. doi: 10.1148/rg.317115074.

14. UCSF Department of Radiology and Biomedical Imaging [Internet]. San Fancisco: UCSF; 2022 [cited 2022 Mar 29]. How to prepare for a Hysterosalpingogram (HSG) procedure. Available from: https://radiology.ucsf.edu/patient-care/prepare/hysterosalpingogram.

15. Radiologyinfo.org for patients [Internet]. RSNA; 2022 [cited 2022 Mar 29]. Hysterosalpingography. Available from:https://www.radiologyinfo.org/en/info/hysterosalp.

16. Costantini-Ferrando MF.What should I expect during a Hysterosalpingogram HSG Test?. 2022 [cited 2022 Mar 29]. In: RMA Location Doctors Education Science Resources Blog [Internet]. RMA Network. [2022]. Available from: https://rmanetwork.com/blog/expect-hysterosalpingogram-hsg/.

17. Kahyaoglu S, Yumusak OH, Kahyaoglu I, Kucukbas GN, Esercan A, Tasci Y. Evaluation of time lapse for establishing distal tubal occlusion diagnosis during hysterosalpingography procedure performed by using water soluble contrast media. J Chinese Med Assoc 2017;80:313-8. doi: 10.1016/j.jcma.2016.09.006.

18. Handelzalts JE, Levy S, Peled Y, Binyamin L, Wiznitzer A, Goldzweig G, et al. Information seeking and perceptions of anxiety and pain among women undergoing hysterosalpingography. Eur J Obstet Gynecol Reprod Biol 2016;202:41-4. doi: 10.1016/j.ejogrb.2016.04.037.

19. Jain S, Inamdar DB, Majumdar A, Jain DK. Effectiveness of paracervical block for pain relief in women undergoing hysterosalpingography. J Hum Reprod Sci 2016;9:230-5. doi: 10.4103/0974-1208.197643.

20. Liberty G, Gal M, Mazaki E, Eldar-Geva T, Vatashsky E, Margalioth EJ. Pain relief of hysterosalpingography by prior uterine cervical application of lidocaine/prilocaine cream. Fertil Steril 2005;84(Suppl 1):127–8.

21. Ahmad G, Duffy J, Watson AJ. Pain relief in hysterosalpingography. Cochrane Database Syst Rev 2007;18:CD006106. doi: 10.1002/14651858.CD006106.pub2.

22. Robinson RD, Casablanca Y, Pagano KE, Arthur NA, Bates GW, Propst AM. Intracervical block and pain perception during the performance of a hysterosalpingogram: A randomized controlled trial. Obstet Gynecol 2007;109:89–93. doi: 10.1097/01.AOG.0000247645.52211.41.

THE ASEAN JOURNAL OF RADIOLOGY
ISSN 2672-9393

23. Anserini P, Delfino F, Ferraiolo A, Remorgida V, Menoni S, De Caro G. Strategies to minimize discomfort during diagnostic hysterosalpingography with disposable balloon catheters: A randomised placebo controlled study with oral nonsteroidal premedication. Fertil Steril 2008;90:844–8. doi: 10.1016/j.fertnstert.2007.07.1302.

24. Tur-Kaspa I, Seidman DS, Soriano D, Greenberg I, Dor J, Bider D. Hysterosalpingography with a balloon catheter versus a metal cannula: a prospective, randomized, blinded comparative study. Human Reprod 1998;13:75–7. doi: 10.1093/humrep/13.1.75.

25. Ayida G, Kennedy S, Barlow D, Chamberlain P. A comparison of patient tolerance of hysterosalpingography-contrast sonography (HyCoSy) with Echovist-200 and X-ray hysterosalpingography for outpatient investigation of infertile women. Ultrasound Obstet Gynecol 1996;7:201–4. doi: 10.1046/j.1469-0705.1996.07030201.x.

26. Ricci G, Guastalla P, Ammar L, Cervi G, Guarnieri S, Sartore A. Balloon catheter vs. cervical vacuum cup for hysterosalpingography: a prospective, randomized, single-blinded study. Fertil Steril 2007;87:1458-67.doi:10.1016/j.fertnstert.2006.11.096.

27. Lindheim SR, Sprague C, Winter TC 3rd. Hysterosalpingography and Sonohysterography: Lessons in Technique. AJR Am J Roentgenol 2006;186: 24–9. doi: 10.2214/ajr.05.0836.

Original Article

# Correlation of ultrasound attenuation imaging versus MRI proton density fat fraction in non-alcoholic fatty liver

*Pantajaree Hiranrat, M.Sc.*[(1)]
*Surachate Siripongsakun, M.D.*[(1)]
*Kamonwan Soonklang, M.Sc.*[(2)]
From [(1)] Sonographer school and [(2)]Data Management Unit, HRH Princess Chulabhorn College of Medical Science, Chulabhorn Royal Academy, Bangkok, Thailand.
Address correspondence to S.S.(surachate@yahoo.com)

Received 8 September 2022 ; revised 24 November 2022 ; accepted 26 November 2022
doi:10.46475/aseanjr.v23i3.185

## Abstract

**Background:** Attenuation Imaging (ATI) is a novel method for assessment of hepatic steatosis, based on ultrasound attenuation by calculating attenuation coefficient which increases in the fatty liver condition. The previous published data comparing ATI and Magnetic Resonance Proton Density Fat Fraction (MR-PDFF) has moderate to high correlation coefficient (r=0.66-0.81). However, fatty liver is commonly associated with obesity which may be an influencing factor of the ATI measurement.

**Objective:** The purpose of this study was to evaluate diagnostic accuracy of ATI in non-alcoholic fatty liver disease (NAFLD) compared to MRI-PDFF.

THE ASEAN JOURNAL OF RADIOLOGY
ISSN 2672-9393

**Materials and Methods:** The 62 non-alcoholic fatty liver disease (NAFLD) patients with available ATI, MRI-PDFF, and MRE examination, excluding cirrhosis, history of significant alcohol drinking, and chronic liver condition were retrospectively evaluated.

**Results:** The correlation coefficient (r) of ATI vs MRI-PDFF were in moderate correlation ($r = 0.63$-$0.69$, $p<0.001$). The inter-observer reliability of two observers was 100% with the Cohen kappa coefficient of 1.00 ($p < 0.001$). Area under the receiver operating characteristics of ATI for diagnosis of steatosis grade > 0 was 0.96 and for diagnosis of steatosis grade > 1 was 0.83.

**Conclusions:** ATI is a novel ultrasound method to quantify the degree of fat deposition with a moderate correlation to MRI-PDFF with high interobserver' reliability. Obesity commonly associated with fatty liver may be an interfering factor of ATI measurement.

**Keywords:** Attenuation imaging, Fatty liver, Steatosis, MRI-PDFF, MRE, NAFLD.

## Introduction

Non-alcoholic fatty liver disease (NAFLD), the most common chronic liver disease worldwide, is increasing rapidly in terms of prevalence, estimated to be 25.24%, 20-30%, and 9.26% in the world, Western countries, and Asia, respectively [1,2]. NAFLD is associated with metabolic risk factors including obesity, insulin resistance and hyperlipidemia. The estimated prevalence of NAFLD in obese people, defined as those who have the body mass index (BMI) >25 kg/m$^2$, hyperlipidemia, and diabetic patients have been reported to be 67%- 94%, 50%, and 70%, respectively [3-7].

The excessive accumulation of triglyceride in the hepatocyte in NAFLD patients, could induce inflammation, leading to non-alcoholic steatohepatitis (NASH)

and clinically significant fibrosis which eventually progresses to hepatic cirrhosis and potentially develops into hepatocellular carcinoma (HCC) [1]. Although the degree of fibrosis is reported to be related to mortality, significant steatosis is found to associate with fibrosis progression in NAFLD [8]. Unlike the cirrhotic stage, NAFLD and early-stage NASH are considered reversible with proper treatment and lifestyle modification [9]. Hence, the ability to early detect and begin treatment monitoring are crucial steps to prevent disease progression to irreversible liver cirrhosis.

Liver biopsy is the gold standard for diagnosing and grading hepatic steatosis, inflammation and fibrosis. However, this procedure is invasive and still has some disadvantages and complications, including sampling error, bleeding, and infection [10]. To overcome these limitations, non-invasive imaging methods have been developed as surrogate methods such as magnetic resonance imaging proton density fat fraction (MRI-PDFF), computed tomography (CT), controlled attenuation parameter (CAP), and conventional ultrasound [11].

MRI-PDFF is an accepted non-invasive standard method to quantify fat using chemical-shift imaging (CSI), which has been reported by earlier studies to have excellent correlation with liver biopsy in detection and grading hepatic steatosis [12]. Some studies also demonstrate that MRI-PDFF can be used to evaluate treatment response for NAFLD in the clinical trials [13-15]. Since this method is expensive and not wildly available, it is not practical to perform MRI-PDFF as a screening tool in large population.

Non-contrast enhanced CT scan is a method to assess hepatic steatosis, using attenuation values to interpret fat component in hepatocytes [16]. This method has high sensitivity and specificity in detection of significant fatty liver > 30% steatosis, limiting the detection of mild steatosis. Radiation exposure is also a main limitation for monitoring purpose [17].

CAP is a non-invasive method based on ultrasound properties, which is implemented in the FibroScan®(Echosens, Paris, France). This method is reported

THE ASEAN JOURNAL OF RADIOLOGY
ISSN 2672-9393

to have high diagnostic accuracy to detect histologically diagnosed hepatic steatosis [11, 18, 19]. Still, some factors such as skin to liver capsule distance, technical error related to operator, invalid value, intolerable pain, and undetectable liver could lower the accuracy rate [20]. Furthermore, the CAP technique is a dedicated measurement method that does not provide hepatic imaging information; therefore, surveillance of other liver conditions cannot be accessed using this method alone.

Conventional ultrasound is widely used for the screening hepatic steatosis, owing to the inexpensiveness and availability. Bright liver score, a semi-quantitative scale, is used to grade hepatic steatosis by comparing liver parenchymal echogenicity to the kidney and wall of hepatic vessels [21]. Many studies reported a good correlation between bright liver score and liver biopsy in the detection of hepatic steatosis [22, 23]. However, in patients with mild steatosis, the accuracy of this method is dramatically decreased [24], impeding the detection of early NAFLD [25].

To overcome the conventional ultrasound limitations, the novel technique implemented in the ultrasound system for assessment of hepatic steatosis based on ultrasound attenuation properties has been developed. Attenuation imaging (ATI; Canon Medical Systems Corporation, Otawara, Tochigi, Japan) is a potential tool for quantifying fat in the liver by calculating the attenuation coefficient of ultrasound in liver tissue, presuming that higher fat composition will increase ultrasound attenuation. ATI can be performed by defining the region of interest (ROI) for attenuation measurement with ultrasound imaging. This method eliminates the interfering factors including time gain compensation and beam focusing in order to receive simple signal intensity profile of the sound to calculate attenuation coefficient of the liver [26, 27].

Several published data, regarding ATI, have shown positive results. A few recent studies claimed a moderate to high correlation between ATI and MRI-PDFF with correlation coefficient = 0.66-0.81, $p<0.001$). Tada et al, reported a good performance of ATI, as compared to liver biopsy, with the diagnostic accuracy

between 76.4-85.1% and area under the receiver operating characteristic curve (AUROC) between 0.85-0.91. However, in the subgroup of the obese patients, the diagnostic accuracy drops from 76-85% to 58-68% in significant fatty liver (grade ≥ 2) [26]. According to recent information, ATI could potentially be another non-invasive method to quantitatively evaluate hepatic steatosis with the need of more data validation, especially in obese population.

The purpose of this study was to investigate the diagnostic capability and correlations of ATI, comparing with MRI-PDFF for detection and staging of hepatic steatosis in NAFLD patients, focusing on obese patients.

## Materials and methods

### Study design and population

This retrospective study was approved by the Ethics Committee for Human Research of the Chulabhorn Research Institute (Certificate number 071/2562). This was undertaken to follow the international ethical guideline and Declaration of Helsinki patients. Informed consent was waived.

All consecutive non-alcoholic fatty liver disease patients who underwent MR elastography, MRI-PDFF with available ATI information at Chulahborn hospital from August to October 2019 were included.

Information of clinical evaluation for fatty liver, basic anthropometric examination, fasting biochemical tests including serum aspartate aminotransferase (AST), alanine aminotransferase (ALT), Triglyceride (TG), Cholesterol and Platelet values were collected. Inclusion criteria were (i) patients at the age of 18 or above (ii) patients who were clinically diagnosed as having the non-alcoholic fatty liver disease (NAFLD) defined by elevated ALT ( ≥ 40 U/L) with liver sonography findings suggestive of fatty liver. Exclusion criteria included (i) known cirrhosis (ii)

THE ASEAN JOURNAL OF RADIOLOGY
ISSN 2672-9393

daily alcohol drinking > 30 g in men, 20 g in women (iii) chronic viral hepatitis B, C, and other known chronic liver diseases such as autoimmune hepatitis, primary biliary cholangitis, etc.

**ATI Evaluation technique**

All patients who underwent conventional gray-scale US and ATI examinations were performed by two operators (S.S. and P.H.) with 12 and 3 years of experience in abdominal US imaging, respectively. Both operators were blinded to the patients' clinical details as well as MRI-PDFF and laboratory results. Liver sonography and ATI examinations were performed using an ultrasound scanner (Aplio i800, Canon Medical Systems, Otawara, Japan) with a 1-8 MHz multi-frequency convex probe. All patients who underwent ATI had fasted for at least 6 hours before examination. All images were obtained in the supine position and the intercostal approach.

For attenuation coefficient measurement of ATI, a 2x4 cm fixed measurement region of interest (ROI) was placed in the middle of the attenuation coefficient map (26). The included ROI was placed on the liver parenchyma, avoiding internal vessels, with the upper margin at least 2 cm below the liver capsule (Figure 1).

The degree of attenuation was color-coded and displayed in the sampling box of ATI. The resulting attenuation coefficient was displayed in the units of dB/cm/MHz. Automated linear regression comparing the observed and the expected values by the machine was represented as $R^2$ values, which are classified as poor ($R^2 < 0.80$), good ($R^2 = 0.80$-$0.89$), or excellent ($R^2 \geq 0.90$) [28].

For the evaluation of inter-observer reliability, the assessment was conducted in a series of 18 subjects. Two operators (S.S. and P.H) performed two sets of 5 ATI measurements on the same subject by an alternating set of measurements between two operators. Measured attenuation coefficient will be categorized into steatosis grade S1, S2, and S3 using cut off level at 0.63, 0.72, 0.75 cm/dB/MHz, respectively according to prior published studies [26-29].

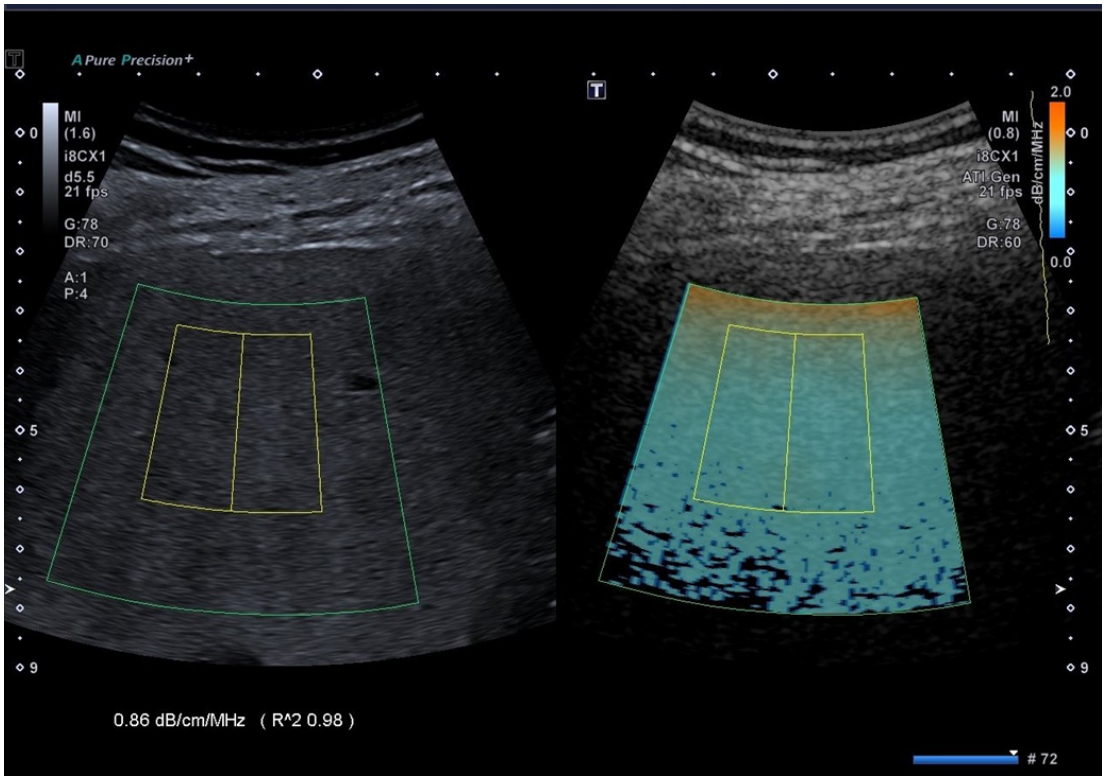


**Figure 1.** *The green box in the right image shows the attenuation color map of ROI (region of interest). The upper margin of the ROI should be about 2 cm below the liver capsule. The measurement area, a yellow box of a fixed 4X2cm as shown in the right image, should be placed at the center of ROI, avoiding major vasculatures.*

## MRI-PDFF and MR elastography

MRI-PDFF and MRE are incorporated into the routine MRI protocol to assess hepatic steatosis and fibrosis in NAFLD patients. MRI was performed with 3.0 Tesla (Ingenia; Philips Healthcare, Best, Netherlands) Protocol of MR-PDFF and MRE are shown in Table 1.

THE ASEAN JOURNAL OF RADIOLOGY
ISSN 2672-9393

**Table 1.** *MRI technique for MRI proton density fat fraction and MR elastography.*

| Parameter | MRI-PDFF | MRE |
|---|---|---|
| Pulse sequence | FSPGR | GRE |
| Matrix | 300x300 | 300x85 |
| No. of signal acquired | 1 | 1 |
| Echo time (msec) | 5.9 | 20 |
| Repetition time (msec) | 1.05 | 50 |
| Delta echo time (msec) | 0.7 | - |
| Flip angle (deg) | 5 | 30 |
| Bandwidth (kHz) | - | 287 |
| No. of sections | 64 | 4 |
| Section thickness (mm) | 5 | 10 |
| Section gab (mm) | 10 | 1 |
| No. of phases | - | 4 |
| MEG frequency (Hz) | - | 60 |
| Axis of MEG | - | Z |
| Driver frequency (Hz) | - | 60 |
| Driver cycles per trigger | - | 3 |
| No. of breath holds | 1 | 4 |
| Breath hold mode | Expiration | Expiration |
| Acceleration factor | - | 2 |
| Imaging time | 7 sec | 1.10 min |
| mDIXON images | Water, fat, fat fraction, T2* | - |

Percentage fat fraction measurement on the MRI-PDFF was performed using a 3x3 cm ROI at the parenchyma of the left lateral hepatic lobe, right anterior, and posterior of the right hepatic lobe, respectively (Figure 2).

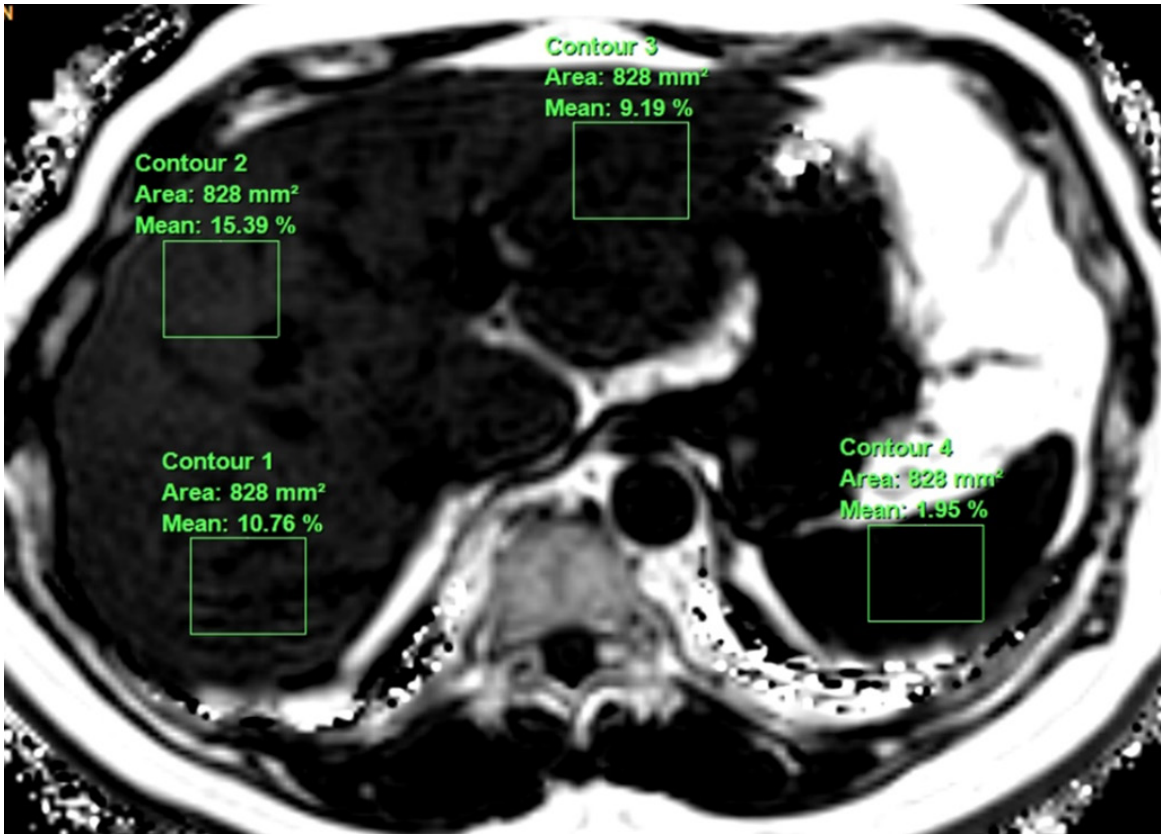


**Figure 2.** *Fast-spoiled gradient echo MR image of fat mapping image, showing measurement area including the posterior segment of the right hepatic lobe (contour 1), the anterior segment of the right hepatic lobe (contour 2), the left hepatic lobe (contour 3), and the spleen (contour 4).*

Quantification of liver fat was categorized by MRI-PDFF as follows; ≥5% (S ≥1: steatosis), ≥16.3% (S≥2: significant steatosis), and ≥21.6% (S≥3: severe steatosis) [30], and MRE was categorized into fibrosis stage f1-f2, f2-f3, f3-f4 and f4 at the cut off value 2.9–3.5 kPa, 3.5–4.0 kPa, 4.0–5.0 kPa, >5.0 kPa respectively [31].

THE ASEAN JOURNAL OF RADIOLOGY
ISSN 2672-9393

**Statistical analysis**

Demographic and anthropometric data of the patients, including age, gender, Body mass index (BMI), and liver function test were evaluated using independent t-test and Mann-Whitney U test to compare demographic data.

The univariate r coefficient was tested to compare ATI and MRI-PDFF using the Spearman rank correlation method and categorized as follows: 0.00-0.25 none or slight; 0.26 to 0.50 fair to moderate; 0.51-0.75 moderate to good; 0.76-1.00; almost perfect [32].

The diagnostic performance of ATI was evaluated by using receiver operation characteristic (ROC) curves and the area under the ROC (AUROC) curves analysis along with Youden index to optimal cut-off value, sensitivity and specificity [33].

The concordance between inter-observer was assessed by Cohen's kappa coefficient, whose results could be interpreted as follows; 0 as an agreement equivalent to chance; 0.01-0.20 as slight agreement; 0.21-0.40 as fair agreement; 0.41-0.60 as moderate agreement; 0.61-0.80 as substantial agreement; 0.81-0.90 as near perfect agreement; 1.00 as a perfect agreement [34]. Analyses were conducted using STATA version 12; Stata Corporation, College Station, Tx) at 2 sided p-value $< 0.05$ as the level of significance.

## Results

There were 62 patients; two patients were excluded due to incomplete data of ATI. Of all patients, average BMI and percentage of patient BMI $\geq 25$ kg/m$^2$ were 27.4 kg/m$^2$, and 72%, respectively. None of the patients had significant liver fibrosis with the stiffness mean of 2.1±0.4 kPa.

The characteristics of all 62 patients (31 women and 31 men), including gender, weight, height, BMI, liver stiffness, serum aspartate aminotransferase (AST), alanine aminotransferase (ALT), fasting blood glucose (FBG), triglycerides (TG), cholesterol (CHOL), and platelet count (PLT) are summarized in Table 2.

**Table 2.** *Demographic data of patients.*

| | Female (n=31) | Male (n=31) | All patients (n=62) | p-value* |
|---|---|---|---|---|
| Age (mean ± SD) | 54.8±10.6 | 46.9±11.1 | 50.9±11.5 | 0.0054* |
| Weight (kg) | 70.4±8.5 | 78.2±10.6 | 74.3±10.4 | 0.0022* |
| Height (cm) | 159.5±6.6 | 170.0±4.1 | 164.8±7.6 | <0.001* |
| Waist circumference (cm) | 92.8±6.1 | 97.8±7.0 | 95.8±7.0 | 0.0255* |
| BMI (kg/m2) | 27.7±3.5 | 27.1±3.4 | 27.4±3.4 | 0.4418 |
| < 25 | 8 (25.8%) | 8 (25.8%) | 16 (25.8%) | - |
| ≥ 25 | 23 (74.2%) | 23 (74.2%) | 46 (74.2%) | - |
| Stiffness* (kPa) | 2.0±0.4 | 2.2±0.3 | 2.1±0.4 | 0.107 |
| | | | | |
| Baseline Laboratory values (mean ± SD) | | | | |
| AST (IU/L) | 34.9±20.5 | 28.2±6.2 | 30.9±14.0 | 0.750 |
| ALT (IU/L) | 49.7±27.5 | 48.5±19.4 | 49.0±22.7 | 0.499 |
| FBG (mg/dL) | 114.4±42.2 | 98.2±21.9 | 104.7±32.1 | 0.0323* |
| TG (mg/dL) | 123.3±45.4 | 146.0±83.4 | 136.9±70.9 | 0.525 |
| CHOL (mg/dL) | 190.0±43.0 | 194.5±31.2 | 192.7±35.9 | 0.294 |
| Plt(x10^3/ul) | 298.1±58.2 | 266.6±51.3 | 279.2±55.7 | 0.122 |

*Stiffness* (kPa) by MR scanner 3.0 Tesla (Ingenia; Philips Healthcare, Best, Netherlands) with MRE protocol*

The correlation of ATI vs MRI-PDFF values at the lateral segment of the left lobe, the anterior and posterior of right hepatic lobe, and average value correlation of ATI vs MRI-PDFF showed a moderate correlation with the highest correlation of the right posterior segment. ($r = 0.63$, $p < 0.001$, $r = 0.66$, $p < 0.001$; $r = 0.69$, $p < 0.001$, $r = 0.67$, $p < 0.001$; respectively) (Figure 3A-D).

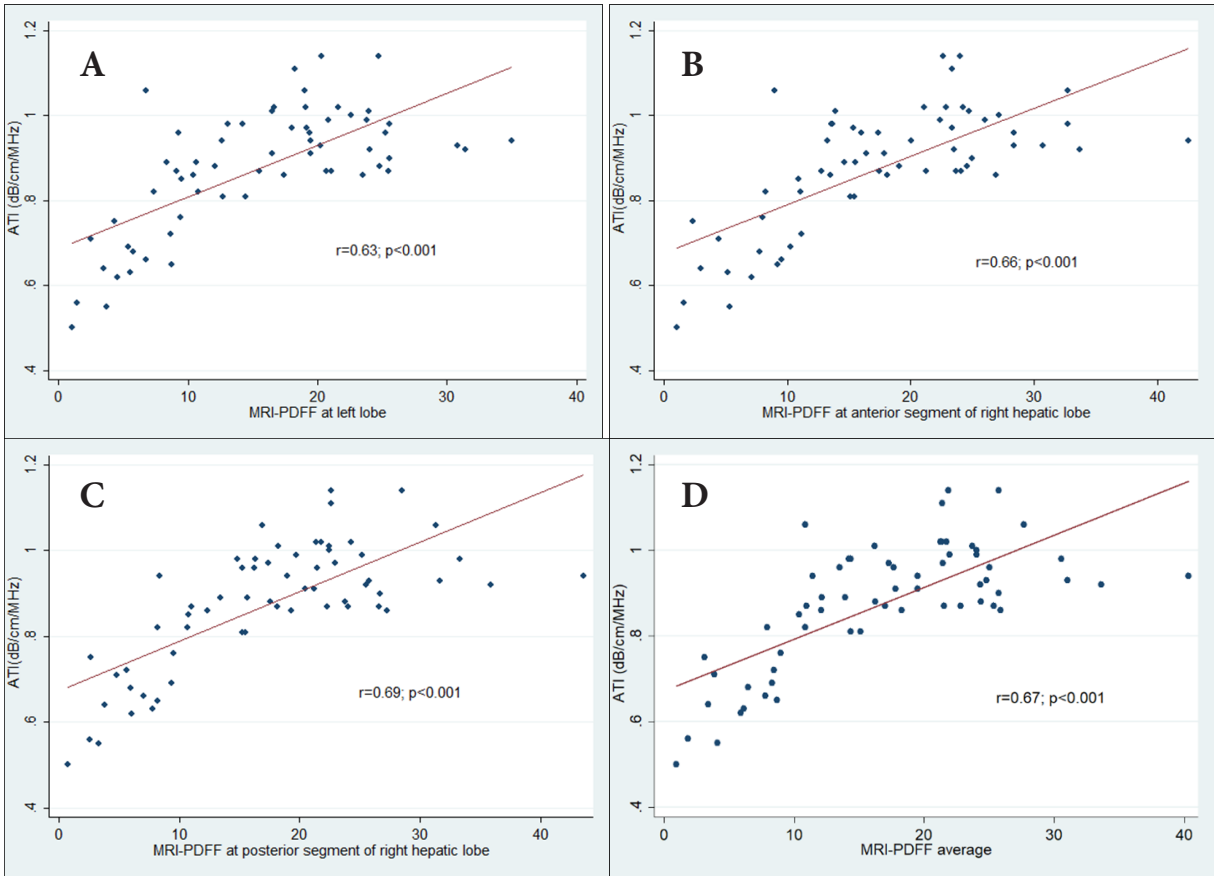


**Figure 3.** *The Spearman's correlation analysis between ATI of liver and MRI-PDFF of different hepatic areas and the average MRI-PDFF value (a) left lobe liver (r = 0.63). (b) anterior segments of right hepatic lobe (r = 0.66). (c) posterior segments of right hepatic lobe (r = 0.69). (d) average value of different hepatic areas (r = 0.67).*

The AUROC value for diagnosis of steatosis grade > 0 was 0.96 using a cutoff point of 0.72 dB/cm/MHz with 89.3% of sensitivity and 83.3% of specificity. The AUROC value for diagnosis of steatosis grade > 1 was 0.83 using a cutoff point of 0.88 dB/cm/MHz with 81.8% of sensitivity and 72.4% of specificity (Figure 4A-B).

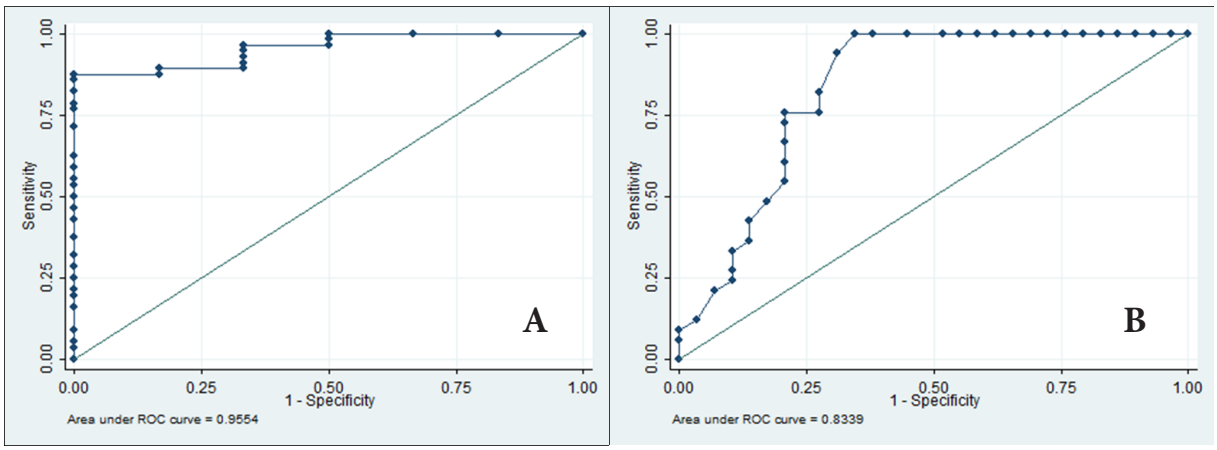


**Figure 4.** *The receiver operation characteristic (ROC) curve for (a) diagnosis of steatosis grade > 0 and (b) grade > 1.*

The agreement of the inter-observer reliability of two observers was 100% with the Cohen kappa coefficient of 1.00 ($p < 0.001$) (Figure 5).

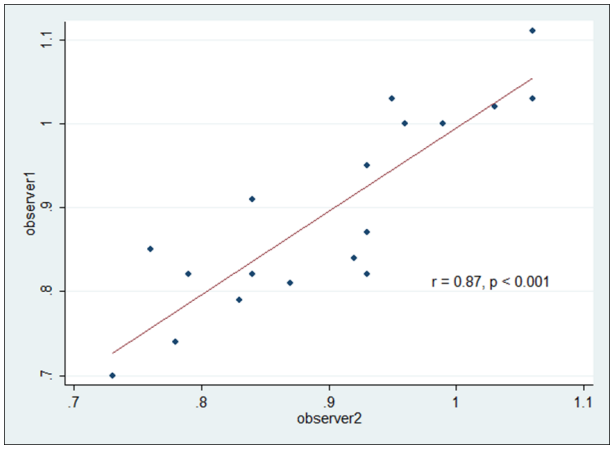


**Figure 5.** *Correlation of ATI measurements between two operators.*

THE ASEAN JOURNAL OF RADIOLOGY
ISSN 2672-9393

## Discussion

MRI-PDFF, a complex based gradient echo sequence with a low flip angle, is a non-invasive biomarker method for the estimated fat concentration of the entire liver [13, 35]. MRI-PDFF is suited for baseline assessment and monitoring of hepatic steatosis after treatment, because of the high correlation between MRI-PDFF and the grading of hepatic steatosis on liver biopsy [13, 35, 36]. However, MRI-PDFF is costly, with limited availability, and requires extra visit in addition to the routine US liver surveillance.

The liver bright score has been commonly used for fatty liver grading using the renal cortex and internal hepatic vascular wall echogenicity as internal references. However, liver bright score is a semi-qualitative evaluation and has certain limitations for follow up indications since the liver bright score grading has a wide range of percentage of fat composition; for example, liver bright score of 1 corresponds to the percentage of about 5-33% of fat. Therefore, subtle changes in the degree of hepatic steatosis will not change in grading on the liver bright score [37]. Besides, the bright liver score may have operator-dependent factors which results in variation in performance [22, 23, 38-41].

ATI is a novel method that has the basic concept of sound attenuation measurement based on fatty tissue that should have higher sound attenuation compared to normal liver tissue [42]. Measurement of attenuation coefficient allows quantitative measurement in addition to the conventional US imaging and potential for follow up indication.

In our study, the correlation coefficient value of ATI with MRI-PDFF was concordant with previously published studies with a slightly lower correlation coefficient of r = 0.63–0.69 compared to r = 0.66–0.81 [27, 29]. This may be explained by the fact that ATI provides real-time grayscale image correlation during the measurement. Furthermore, ATI provides color mapping for the degree of attenuation and coefficient of determination ($R^2$) for optimal ROI placement [43, 44]. However, there are potential interfering factors of the ATI

measurement which may cause less reliability. Jeon et al. have found that the patients with the skin-to-liver distance greater than 20 mm had significantly less correlation between ATI and MRI-PDFF [27].

The majority of studies comparing ATI and MRI-PDFF have limited data on S3 patients [26, 29]. Tada et al. found less specificity and AUROC of ATI in categorizing the steatosis stage of the NAFLD patients as compared with other groups of patients. Tada et al. reported the subgroup of higher grading of fatty liver tends to have less diagnostic performance [26]. Our study may substantiate these interfering factors since 75% of our population have BMI of over 25 and all patients are diagnosed with fatty liver. ATI is less reliable in an obese patient, which is possibly due to the deeper the sound passing through, the greater attenuation, resulting in higher attenuation coefficient [45]. Obese patients presumably have the thicker abdominal wall and preperitoneal fat which increases the distance between the transducer and the measurement area. This factor may interfere with ATI measurement, causing decreased correlation.

Overall, the ATI value shows a better correlation to MRI-PDFF at the right posterior hepatic lobe as compared with other locations. This could be explained by the technique of ATI measurement at the right intercostal approach, mainly representing the posterior right hepatic lobe. Therefore, the correlation of ATI is more concordant with the measurement of fat at the right posterior hepatic lobe than other places.

ATI may have limitations in the sampling area which is mainly measured in right hepatic lobe; however, fatty liver is a diffuse process which involves the entire liver parenchyma. Thus, MRI-PDFF is still more suitable for evaluation of the whole liver.

Perfect interobserver reliability (k=1.0) in grading liver steatosis is observed in our study, which is maybe because ATI is relatively non-complicated to use with fix measurement ROI box, and measurable area. Jeon et al. also reported high reliability in both interobserver and intraobserver (k 0.8-1.0) [27]. With this

THE ASEAN JOURNAL OF RADIOLOGY
ISSN 2672-9393

high reproducibility, ATI may be a good alternative method for monitoring the treatment of NAFLD.

There were a few limitations in this study. First of all, this study was a retrospective study resulting in uncontrolled protocols and operators at the beginning. Second, the number of S2 and S3 patients were too small to analyze.

## Conclusion

In this regard, ATI equipped in the US system allows additional quantitative measurement of liver steatosis in the same setting of liver US study. ATI may potentially be a surrogate method to evaluate and assess the degree of fatty liver in the routine clinical setting.

## References

1. Younossi ZM, Koenig AB, Abdelatif D, Fazel Y, Henry L, Wymer M. Global epidemiology of nonalcoholic fatty liver disease-Meta-analytic assessment of prevalence, incidence, and outcomes. Hepatology 2016;64:73-84. doi: 10.1002/hep.28431.

2. Sayiner M, Koenig A, Henry L, Younossi ZM. Epidemiology of Nonalcoholic Fatty Liver Disease and Nonalcoholic Steatohepatitis in the United States and the Rest of the World. Clin Liver Dis 2016;20:205-14. doi: 10.1016/j.cld.2015.10.001.

3. Argo CK, Caldwell SH. Epidemiology and natural history of non-alcoholic steatohepatitis. Clin Liver Dis 2009;13:511-31. doi: 10.1016/j.cld.2009.07.005.

4. Bellentani S, Bedogni G, Miglioli L, Tiribelli C. The epidemiology of fatty liver. Eur J Gastroenterol Hepatol 2004;16:1087-93. doi: 10.1097/00042737-200411000-00002.

5. Assy N, Kaita K, Mymin D, Levy C, Rosser B, Minuk G. Fatty infiltration of liver in hyperlipidemic patients. Dig Dis Sci 2000;45:1929-34. doi: 10.1023/a:1005661516165.

6. Wu KT, Kuo PL, Su SB, Chen YY, Yeh ML, Huang CI, et al. Nonalcoholic fatty liver disease severity is associated with the ratios of total cholesterol and triglycerides to high-density lipoprotein cholesterol. J Clin Lipidol 2016;10: 420-5 e1. doi: 10.1016/j.jacl.2015.12.026.

7. Targher G, Bertolini L, Padovani R, Rodella S, Tessari R, Zenari L, et al. Prevalence of nonalcoholic fatty liver disease and its association with cardiovascular disease among type 2 diabetic patients. Diabetes Care 2007;30:1212-8. doi: 10.2337/dc06-2247.

8. Ajmera V, Park CC, Caussy C, Singh S, Hernandez C, Bettencourt R, et al. Magnetic Resonance Imaging Proton Density Fat Fraction Associates With Progression of Fibrosis in Patients With Nonalcoholic Fatty Liver Disease. Gastroenterology 2018;155:307-10 e2. doi: 10.1053/j.gastro.2018.04.014.

9. Lackner C. Hepatocellular ballooning in nonalcoholic steatohepatitis: the pathologist's perspective. Expert Rev Gastroenterol Hepatol 2011;5:223-31. doi: 10.1586/egh.11.8.

10. Rockey DC, Caldwell SH, Goodman ZD, Nelson RC, Smith AD; American Association for the Study of Liver Diseases. Liver biopsy. Hepatology 2009;49:1017-44. doi: 10.1002/hep.22742.

THE ASEAN JOURNAL OF RADIOLOGY
ISSN 2672-9393

11. Chon YE, Jung KS, Kim SU, Park JY, Park YN, Kim DY, et al. Controlled attenuation parameter (CAP) for detection of hepatic steatosis in patients with chronic liver diseases: a prospective study of a native Korean population. Liver Int 2014;34:102-9. doi: 10.1111/liv.12282.

12. Cassidy FH, Yokoo T, Aganovic L, Hanna RF, Bydder M, Middleton MS, et al. Fatty liver disease: MR imaging techniques for the detection and quantification of liver steatosis. Radiographics 2009;29:231-60. doi: 10.1148/rg.291075123.

13. Middleton MS, Heba ER, Hooker CA, Bashir MR, Fowler KJ, Sandrasegaran K, et al. Agreement Between Magnetic Resonance Imaging Proton Density Fat Fraction Measurements and Pathologist-Assigned Steatosis Grades of Liver Biopsies From Adults With Nonalcoholic Steatohepatitis. Gastroenterology 2017;153:753-61. doi: 10.1053/j.gastro.2017.06.005.

14. Le TA, Chen J, Changchien C, Peterson MR, Kono Y, Patton H, et al. Effect of colesevelam on liver fat quantified by magnetic resonance in nonalcoholic steatohepatitis: a randomized controlled trial. Hepatology 2012;56:922-32. doi: 10.1002/hep.25731.

15. Cui J, Philo L, Nguyen P, Hofflich H, Hernandez C, Bettencourt R, et al. Sitagliptin vs. placebo for non-alcoholic fatty liver disease: A randomized controlled trial. J Hepatol 2016;65:369-76. doi: 10.1016/j.jhep.2016.04.021.

16. Li Q, Dhyani M, Grajo JR, Sirlin C, Samir AE. Current status of imaging in nonalcoholic fatty liver disease. World J Hepatol 2018;10:530-42. doi: 10.4254/wjh.v10.i8.530.

17. Park SH, Kim PN, Kim KW, Lee SW, Yoon SE, Park SW, et al. Macrovesicular hepatic steatosis in living liver donors: use of CT for quantitative and qualitative assessment. Radiology 2006;239:105-12. doi: 10.1148/radiol.2391050361.

18. Lee HW, Park SY, Kim SU, Jang JY, Park H, Kim JK, et al. Discrimination of Nonalcoholic Steatohepatitis Using Transient Elastography in Patients with Nonalcoholic Fatty Liver Disease. PLoS One 2016;11:e0157358. doi: 10.1371/journal.pone.0157358.

19. Sasso M, Beaugrand M, de Ledinghen V, Douvin C, Marcellin P, Poupon R, et al. Controlled attenuation parameter (CAP): a novel VCTE guided ultrasonic attenuation measurement for the evaluation of hepatic steatosis: preliminary study and validation in a cohort of patients with chronic liver disease from various causes. Ultrasound Med Biol 2010;36:1825-35. doi: 10.1016/j.ultrasmedbio.2010.07.005.

20. Vuppalanchi R, Siddiqui MS, Van Natta ML, Hallinan E, Brandman D, Kowdley K, et al. Performance characteristics of vibration-controlled transient elastography for evaluation of nonalcoholic fatty liver disease. Hepatology 2018;67:134-44. doi: 10.1002/hep.29489.

21. Ricci C, Longo R, Gioulis E, Bosco M, Pollesello P, Masutti F, et al. Noninvasive in vivo quantitative assessment of fat content in human liver. J Hepatol 1997;27:108-13. doi: 10.1016/s0168-8278(97)80288-7.

22. Palmentieri B, de Sio I, La Mura V, Masarone M, Vecchione R, Bruno S, et al. The role of bright liver echo pattern on ultrasound B-mode examination in the diagnosis of liver steatosis. Dig Liver Dis 2006;38:485-9. doi: 10.1016/j.dld.2006.03.021.

23. Saadeh S, Younossi ZM, Remer EM, Gramlich T, Ong JP, Hurley M, et al. The utility of radiological imaging in nonalcoholic fatty liver disease. Gastroenterology 2002;123:745-50. doi: 10.1053/gast.2002.35354.

24. Shannon A, Alkhouri N, Carter-Kent C, Monti L, Devito R, Lopez R, et al. Ultrasonographic quantitative estimation of hepatic steatosis in children With NAFLD. J Pediatr Gastroenterol Nutr 2011;53:190-5. doi: 10.1097/MPG.0b013e31821b4b61.

THE ASEAN JOURNAL OF RADIOLOGY
ISSN 2672-9393

25. Fitzpatrick E, Dhawan A. Noninvasive biomarkers in non-alcoholic fatty liver disease: current status and a glimpse of the future. World J Gastroenterol 2014;20:10851-63. doi: 10.3748/wjg.v20.i31.10851.

26. Tada T, Iijima H, Kobayashi N, Yoshida M, Nishimura T, Kumada T, et al. Usefulness of Attenuation Imaging with an Ultrasound Scanner for the Evaluation of Hepatic Steatosis. Ultrasound Med Biol 2019;45:2679-87. doi: 10.1016/j.ultrasmedbio.2019.05.033.

27. Jeon SK, Lee JM, Joo I, Yoon JH, Lee DH, Lee JY, et al. Prospective Evaluation of Hepatic Steatosis Using Ultrasound Attenuation Imaging in Patients with Chronic Liver Disease with Magnetic Resonance Imaging Proton Density Fat Fraction as the Reference Standard. Ultrasound Med Biol 2019;45:1407-16. doi: 10.1016/j.ultrasmedbio.2019.02.008.

28. Bae JS, Lee DH, Lee JY, Kim H, Yu SJ, Lee JH, et al. Assessment of hepatic steatosis by using attenuation imaging: a quantitative, easy-to-perform ultrasound technique. Eur Radiol 2019;29:6499-507. doi: 10.1007/s00330-019-06272-y.

29. Ferraioli G, Maiocchi L, Raciti MV, Tinelli C, De Silvestri A, Nichetti M, et al. Detection of Liver Steatosis With a Novel Ultrasound-Based Technique: A Pilot Study Using MRI-Derived Proton Density Fat Fraction as the Gold Standard. Clin Transl Gastroenterol 2019;10:e00081. doi: 10.14309/ctg.0000000000000081.

30. Caussy C, Alquiraish MH, Nguyen P, Hernandez C, Cepin S, Fortney LE, et al. Optimal threshold of controlled attenuation parameter with MRI-PDFF as the gold standard for the detection of hepatic steatosis. Hepatology 2018;67:1348-59. doi: 10.1002/hep.29639.

31. Hoodeshenas S, Yin M, Venkatesh SK. Magnetic Resonance Elastography of Liver: Current Update. Top Magn Reson Imaging 2018;27:319-33. doi: 10.1097/RMR.0000000000000177.

32. Colton T. Statistics in Medicine. Boston: Little, Brown and Company; 1974.

33. Youden WJ. Index for rating diagnostic tests. Cancer 1950;3:32-5. doi: 10.1002/1097-0142(1950)3:1<32::aid-cncr2820030106>3.0.co;2-3.

34. McHugh ML. Interrater reliability: the kappa statistic. Biochem Med (Zagreb) 2012;22:276-82.

35. Caussy C, Reeder SB, Sirlin CB, Loomba R. Noninvasive, Quantitative Assessment of Liver Fat by MRI-PDFF as an Endpoint in NASH Trials. Hepatology 2018;68:763-72. doi: 10.1002/hep.29797.

36. Permutt Z, Le TA, Peterson MR, Seki E, Brenner DA, Sirlin C, et al. Correlation between liver histology and novel magnetic resonance imaging in adult patients with non-alcoholic fatty liver disease - MRI accurately quantifies hepatic steatosis in NAFLD. Aliment Pharmacol Ther 2012;36:22-9. doi: 10.1111/j.1365-2036.2012.05121.x.

37. Saverymuttu SH, Joseph AE, Maxwell JD. Ultrasound scanning in the detection of hepatic fibrosis and steatosis. Br Med J (Clin Res Ed) 1986;292:13-5. doi: 10.1136/bmj.292.6512.13.

38. Hamaguchi M, Kojima T, Itoh Y, Harano Y, Fujii K, Nakajima T, et al. The severity of ultrasonographic findings in nonalcoholic fatty liver disease reflects the metabolic syndrome and visceral fat accumulation. Am J Gastroenterol 2007;102:2708-15. doi: 10.1111/j.1572-0241.2007.01526.x.

THE ASEAN JOURNAL OF RADIOLOGY
ISSN 2672-9393

39. Hepburn MJ, Vos JA, Fillman EP, Lawitz EJ. The accuracy of the report of hepatic steatosis on ultrasonography in patients infected with hepatitis C in a clinical setting: a retrospective observational study. BMC Gastroenterol 2005;5:14. doi: 10.1186/1471-230X-5-14.

40. Mathiesen UL, Franzen LE, Aselius H, Resjo M, Jacobsson L, Foberg U, et al. Increased liver echogenicity at ultrasound examination reflects degree of steatosis but not of fibrosis in asymptomatic patients with mild/moderate abnormalities of liver transaminases. Dig Liver Dis 2002;34:516-22. doi: 10.1016/s1590-8658(02)80111-6.

41. Soresi M, Giannitrapani L, Florena AM, La Spada E, Di Gesaro V, Rappa F, et al. Reliability of the bright liver echo pattern in diagnosing steatosis in patients with cryptogenic and HCV-related hypertransaminasaemia. Clin Radiol 2009;64:1181-7. doi: 10.1016/j.crad.2009.06.013.

42. Culjat MO, Goldenberg D, Tewari P, Singh RS. A review of tissue substitutes for ultrasound imaging. Ultrasound Med Biol 2010;36:861-73. doi: 10.1016/j.ultrasmedbio.2010.02.012.

43. Ferraioli G, Maiocchi L, Savietto G, Tinelli C, Nichetti M, Rondanelli M, et al. Performance of the Attenuation Imaging Technology in the Detection of Liver Steatosis. J Ultrasound Med 2021;40:1325-32. doi: 10.1002/jum.15512.

44. Yoo J, Lee JM, Joo I, Lee DH, Yoon JH, Kang HJ, et al. Reproducibility of ultrasound attenuation imaging for the noninvasive evaluation of hepatic steatosis. Ultrasonography 2020;39:121-9. doi: 10.14366/usg.19034.

45. Kremkau FW. Sonography: Principles and Instruments. 9th ed. Philadelphia: Elsevier; 2016.

Original Article

# Dual-energy spectral CT in assessment of pleural effusion

*Wilailak Muang-im M.D.*[(1)]
*Juntima Euathrongchit M.D.*[(1)]
*Apichat Tantraworasin M.D., Ph.D.*[(2,3)]
*Yutthaphan Wannasopha M.D.*[(1)]
From [(1)] Department of Radiology, [(2)]Clinical Epidemiology and Clinical Statistics Center and Department of Surgery, [(3)]Clinical Surgical Research Center, Faculty of Medicine, Chiang Mai University, Chiang Mai, Thailand.
Address correspondence to Y.W.(email: wyutthaphan@gmail.com)

Received 12 November 2022 ; revised 12 December 2022 ; accepted 17 December 2022
doi:10.46475/aseanjr.v23i3.193

## Abstract

**Background:** Pleural effusion is a common clinical problem. The ability to differentiate between benign and malignant pleural effusions has many clinical benefits. However, few studies have investigated the diagnostic value of dual-energy spectral computed tomography (DECT) in pleural effusion.

**Objective:** To evaluate the diagnostic values of DECT for assessment of pleural effusion.

**Materials and Methods:** We retrospectively analyzed data from 87 patients presenting with pleural effusion who underwent chest DECT from October 2019 to November 2020. Two reviewers blindly reviewed the CT images of pleural effusion in consensus. The pleural fluid attenuation in standard conventional CT images and monoenergetic images, at 40 keV, 100 keV and 140 keV, were recorded.

THE ASEAN JOURNAL OF RADIOLOGY
ISSN 2672-9393

Data pertaining to the effective atomic number, the iodine concentration (IC) and associated CT findings including pleural thickening, pleural nodules and extrapleural fat clouding was analyzed.

**Results:** Of 87 patients, 44 were presented with benign effusions and the remaining 43 were presented with malignancy. There were no statistically significant differences in differentiating between benign and malignant pleural effusions by using the attenuation values, the effective atomic number or the IC. Irregular pleural thickening and pleural nodules were detected statistically significantly in the patients with malignant pleural effusions with moderate accuracy, (48.83%; $p < 0.01$; AuROC 0.7103 and 34.88%; $p < 0.01$; AuROC 0.654 respectively).

**Conclusion:** DECT attenuation values did not show any reliable clinical value in the differentiation between benign and malignant pleural effusions. The presence of pleural nodules or irregular pleural thickening would suggest malignant pleural effusion with moderate accuracy.

**Keywords:** Pleural effusion, Dual energy spectral computed tomography, Benign pleural effusion, Malignant pleural effusion.

## Introduction

Pleural effusion is a common clinical problem consequential to various benign and malignant causes including cardiac problems, malignant tumors, tuberculous pleuritis, and pneumonia. The pleural effusion can be classified into either transudate or exudate. Transudate effusions are caused by imbalances in capillary hydrostatic or colloid oncotic forces. The common causes are usually from cardiac or renal diseases such as heart failure, renal failure, and cirrhosis. However, an exudate effusion generally results from changes in the local factors influencing the accumulation of pleural fluid such as an increase in microvascular permeability, usually due to inflammatory or neoplastic processes [1, 2].

Differentiation between benign and malignant pleural effusions is important as this has an impact on the treatment decision and outcome. Early treatment of benign pleural effusion is curative and decreases the possibility of complications. Likewise, early diagnosis and treatment of malignant pleural effusion may improve the quality of life and increase the survival rate of patients [3].

Diagnostic thoracentesis is the first step in the characterization of a pleural effusion but the examination of pleural fluid cytology only has a sensitivity of about 60% for exclusion of malignancy; therefore, a video-assisted thoracoscopic surgery (VATS)-guided biopsy to confirm diagnosis may be required [1, 4]. However, the VATS is an invasive procedure. The combination of chest CT and pleural fluid cytology improves specificity and sensitivity for facilitating a differential diagnosis between benign and malignant pleural effusions [5].

Nowadays, recent innovations in CT technology have led to the introduction of dual energy spectral CT, the process becoming clinically applicable in enabling better discrimination and characterization of tissues. The dual energy spectral CT can differentiate between material densities by two different energies; low and high-energy images [6]. Dual energy spectral imaging can produce virtual monoenergetic images (40–140 keV) that reduce the beam hardening artifact that affects the CT number and provides a more accurate CT attenuation value than the conventional polychromatic X-ray [7, 8]. Many thousands of dual-energy spectral chest CT scans have been performed each year in our hospital. If dual-energy spectral chest CT can improve the accuracy in differentiation between the benign and malignant pleural effusions, it would be beneficial in avoiding invasive procedures, facilitating early diagnosis and treatment, subsequently improving the quality of life and increasing the survival rate among patients.

To the best of our knowledge, there are few studies investigating the diagnostic value of dual-energy spectral CT in pleural effusion. The objective of this study was to evaluate the diagnostic value of dual-energy spectral chest CT for assessment of pleural effusion.

THE ASEAN JOURNAL OF RADIOLOGY
ISSN 2672-9393

## Materials and methods

### 2.1 Patients

This study was approved by the institutional review board and the written informed consent was waived because of the retrospective nature of the study. This study included 203 patients who underwent dual energy spectral CT of the chest or chest including the abdomen with presence of pleural effusion in our institution between October 2019 and November 2020. One hundred and sixteen patients were excluded from the study. The exclusion criteria were: (1) the nature of pleural effusion was undetermined (96.5%), (2) the amount of pleural effusion was too small to affect the measurement results (1.7%), (3) patients were younger than 18 years old (0.9%), and (4) patients were with unenhanced DECT scans (0.9%). Finally, 87 patients were enrolled into our study. Eligibility criteria for benign pleural effusion were: histopathologic or cytologic confirmation of negativity of malignancy, interval decreased amount of the pleural effusion after follow up imaging and no clinical scenario of malignancy. All of the malignant pleural effusions were verified by pleural fluid cytology or pleural biopsy.

### 2.2 Data collection and image analysis

All patients had undergone dual-energy spectral CT by using the 64-detector row SDCT system (iQon Spectral CT, Philips Healthcare). This system uses a single X-ray tube and a dual-layer detector. The detector separates the X-ray beam into low (upper layer) and high (lower layer) energy data, which is used to reconstruct spectral-based images (SBI). The SBI contain the raw data of both layers and are used to reconstruct any dual-energy images and/or facilitate analysis. The patients were in the supine position. The images were obtained in the craniocaudal direction. Fifty to one hundred ml (350 mg iodine/ml) of the contrast agent were injected through the antecubital vein at a dose of 1 ml/kg of the body weight, injected at a rate of 4.0-4.5 ml/sec. The portovenous phase of scanning was performed at 60-70 seconds after the injection of the contrast medium.

All CT images of pleural effusion were reviewed by two thoracic radiologists with consensus achieved. Post-processing reconstruction CT images use IntelliSpace Portal, version 9.0; Philips software workstation to evaluate the attenuation of pleural effusion in a pre-contrast scan, standard reconstruction conventional post contrast scan, 40 keV monoenergetic image, 100 keV monoenergetic image, 140 keV monoenergetic image, effective atomic number, iodine overlay (IO) image (Figure 1) and associated CT findings including pleural thickening, pleural nodules and extrapleural fat clouding (Figure 2). The pleural thickenings were classified into none, diffuse, irregular or circumferential thickening.

For the quantitative measurements, the area of the region of interest (ROI) ranging from 20 $mm^2$ to 70 $mm^2$ was placed in the center area of the pleural effusion and away from the artifacts (Figure 1). The copy-plate function was used in each patient to ensure equal localization and size. The pleural effusion of each patient has been measured three times in different location in each CT section and averaged to obtain the final result of mean value for attenuation and iodine concentration.

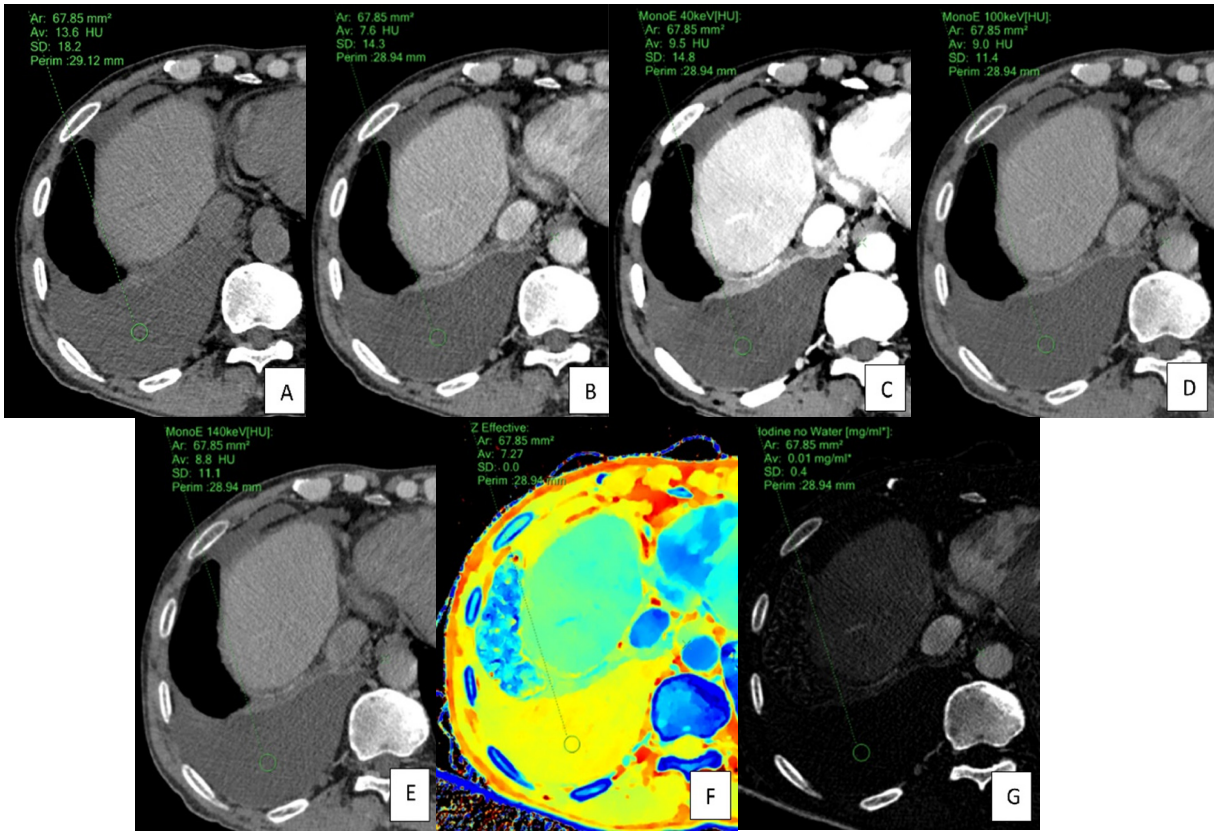


**Figure 1.** *ROI size and location in different images A: pre contrast scan B: standard reconstruction conventional post contrast scan C: 40 keV monoenergetic image D: 100 keV monoenergetic image E: 140 keV monoenergetic image F: effective atomic number G: iodine overlay (IO) image.*

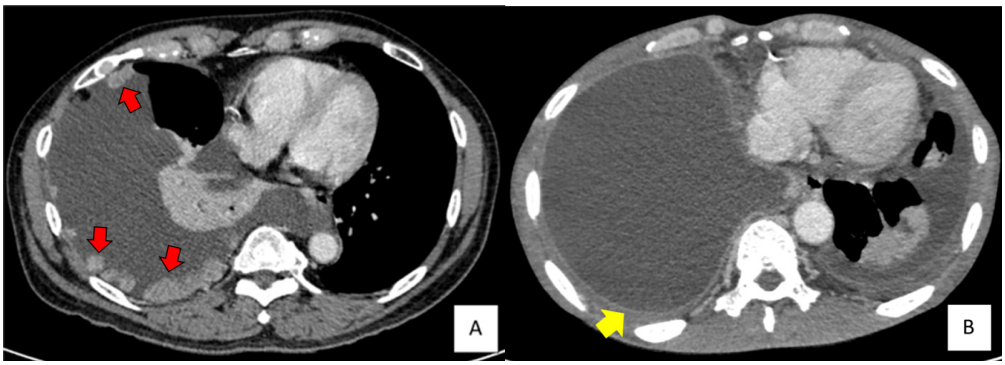


**Figure 2.** *Standard reconstruction chest CT images show multiple enhanced pleural nodules (red arrows) (A) and extrapleural fat clouding (yellow arrow) (B).*

### 2.3 Statistical analysis

Data was statistically analyzed using a programming package for statistics. The results were presented as mean and standard deviation for quantitative variables. Multiple logistic regression analysis was used to compare the various CT findings between benign and malignant pleural effusions. The independent sample student-t test was used to analyze the CT parameters including pre contrast scan, standard reconstruction conventional post contrast scan, 40 keV monoenergetic image, 100 keV monoenergetic image, 140 keV monoenergetic image, effective atomic number, iodine overlay image and associated CT findings including pleural thickening, pleural nodules and extrapleural fat clouding. Factors found to have a p-value $< 0.05$ in the initial analyses were included in the receiver operating characteristic (ROC) analysis. The ROC curves were generated to distinguish benign and malignant pleural effusion. Diagnostic capability was determined by calculating the area under the ROC curve (AuROC). All statistical analyses were performed using SPSS program version 25.

## Results

Our study included 87 patients, divided into two categories including ones with benign effusion and ones shown with malignant effusion groups. The benign group included 44 patients, of whom, 26 were males and 18 were females with an age range of 33 to 79 years (mean age 61.04±11.6 years). The malignant group included 43 patients, of whom, 17 were males and 26 were females with an age range of 32 to 92 years (mean age 65 ±12.2 years). The demographic data of these patients is shown in Table 1.

THE ASEAN JOURNAL OF RADIOLOGY
ISSN 2672-9393

**Table 1.** *Demographic data of patients.*

| Variable | Benign pleural effusion | Malignant pleural effusion | Total |
|---|---|---|---|
| Patients n (%) | 44 (50.57) | 43 (49.43) | 87 (100) |
| Mean age years (SD) | 61.04 (11.6) | 65 (12.2) | 63 (12.0) |
| Gender | | | |
| Female | 18 | 26 | 44 |
| Male | 26 | 17 | 43 |
| Causes of pleural effusions n (%) | TB pleurisy 6 (13.6)<br>Bacterial empyema 7 (15.9)<br>Heart disease 4 (9.1)<br>Unidentified cause 27 (61.4) | Metastatic lung cancer 31(72.1)<br>Metastatic breast cancer 5 (11.6)<br>Metastatic stomach cancer 3 (7.0)<br>Metastatic other tumors 3 (7.0)<br>Primary malignant mesothelioma 1 (2.3) | 87 (100) |

*SD, standard deviation.*

### 3.2 Measurements from spectral CT between benign and malignant pleural effusions

In our study spectral CT based imaging showed no statistically significant difference regards to differentiation between benign and malignant pleural effusions by using the monoenergetic images at every energy level (21.75±11.06 HU vs. 21.37±11.05HU at 40keV, p = 0.873; 13.99±8.55 HU vs. 13.01±5.65 HU at 100keV, p = 0.528; 13.41±8.74 HU vs. 12.40±5.63 HU at 140keV, p = 0.520). Moreover, the standard conventional CT images showed no significant difference between the attenuation values between the benign and malignant pleural effusions in both pre- and post-contrast images (10.79±8.0 HU vs. 12.71±5.33 HU in pre contrast image, p = 0.206; 14.45±7.74 HU vs. 13.45±6.78 HU in post

contrast image, p = 0.523). No significant difference was found in the Z effective atomic number and the iodine concentration for differentiation between the benign and malignant groups (7.32±0.09 vs. 7.33±0.07 of the Z effective atomic number, p = 0.777; 0.13±0.09 vs. 0.12±0.10 mg/ml of the iodine concentration, p = 0.272). A summary of the measurement results is summarized in Table 2. The ROC analysis shown in Figure 3 indicates the inability to differentiate between benign and malignant pleural effusions in all measurement parameters.

**Table 2.** *Comparison of measurements from spectral CT between benign and malignant pleural effusions.*

| Parameter | Benign (N=44) Mean (±SD) | Malignancy (N=43) Mean (±SD) | p-value | AuROC (Std.error) |
|---|---|---|---|---|
| Monoenergetic image (HU) | | | | |
| 40 keV | 21.75 (±11.06) | 21.37 (±11.05) | 0.873 | 0.498 (0.065) |
| 100 keV | 13.99 (±8.55) | 13.01 (±5.65) | 0.528 | 0.497 (0.066) |
| 140 keV | 13.41 (±8.74) | 12.40 (±5.63) | 0.520 | 0.499 (0.066) |
| **Pre contrast conventional image (HU)** | 10.79 (±8.0) | 12.71 (±5.33) | 0.206 | 0.623 (0.062) |
| **Post contrast conventional image (HU)** | 14.45 (±7.74) | 13.45 (±6.78) | 0.523 | 0.466 (0.064) |
| **Effective Atomic Number** | 7.32 (±0.09) | 7.33 (±0.07) | 0.777 | 0.517 (0.065) |
| **Iodine concentration (mg/ml)** | 0.13 (±0.09) | 0.12 (±0.10) | 0.272 | 0.465 (0.065) |

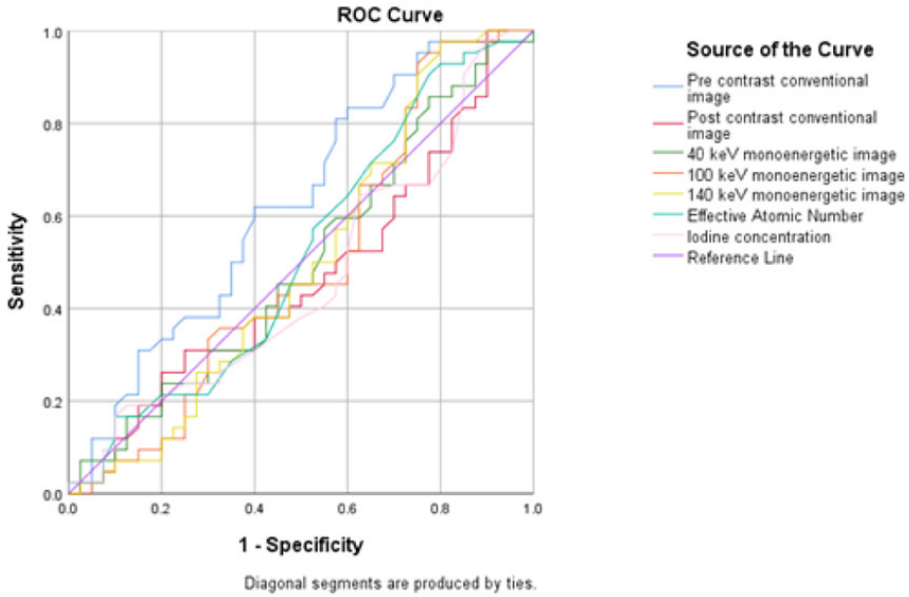


**Figure 3.** *The receiver operating characteristic curve of spectral CT parameters for differentiation between benign and malignant pleural effusions.*

Twenty-five out of 44 benign effusions had no pleural thickening (56.81%) while 14 out of 43 malignant effusions had no pleural thickening (32.55%) ($p = 0.023$). Pleural nodules were observed in 15 out of 43 malignant pleural effusions (34.88%) compared with 2 out of 44 benign pleural effusions (4.54%) ($p < 0.001$) (Figure 4). Of the 44 benign effusions, three showed irregular pleural thickening (6.81%) compared with 21 out of 43 malignant effusions (48.83%) ($p < 0.001$) (Figure 5). A summary of the associated CT findings between benign and malignant pleural effusions is shown in Table 3. There were no significant differences in diffuse pleural thickening, circumferential pleural thickening and extrapleural fat clouding between the two groups. The ROC analysis of pleural nodule and irregular pleural thickening revealed moderate accuracy in differentiating between benign and pleural effusions (AuROC 0.654 and 0.713 respectively) (Figure 6). The multivariate analysis of a combination of pleural nodules and irregular pleural thickening showed slightly increased accuracy in enabling the differentiation between benign and pleural effusions (AuROC 0.761 and standard error 0.053) (Figure 7).

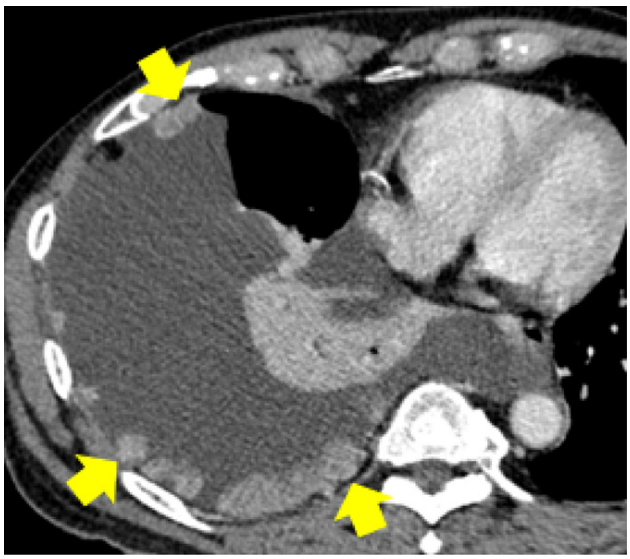

**Figure 4.** *A 66-year old man with lung cancer and right pleural metastasis-standard reconstruction chest CT images show multiple various size enhanced pleural nodules along the right hemithorax (arrows). Also noted large amount of right pleural effusion with adjacent compressive atelectasis of the right lower lobe. atelectasis of the right lower lobe.*

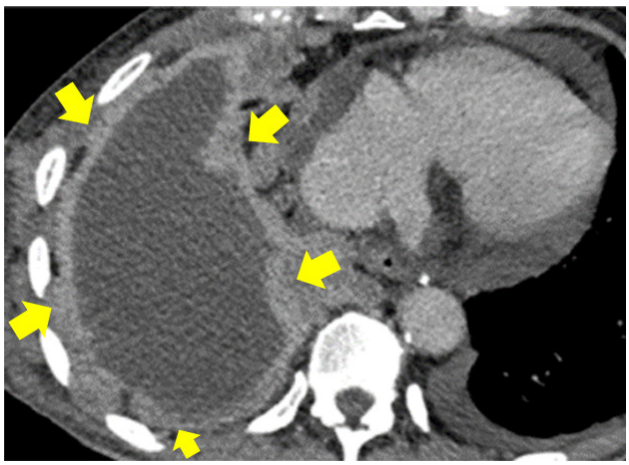

**Figure 5.** *A 70-year-old man with squamous cell lung cancer and right pleural metastasis-standard reconstruction chest CT images show right pleural effusion with subadjacent irregular pleural thickening along the right hemithorax (arrows).*

**Table 3.** *Comparison of the associated CT findings between benign and malignant pleural effusions.*

| CT findings | Benign n=44 n (%) | Malignant n=43 n (%) | p-value | AuROC (Std.error) |
|---|---|---|---|---|
| **Pleural thickening** | | | | |
| No thickening | 25 (56.81) | 14 (32.55) | 0.023 | 0.367 (0.062) |
| Diffuse | 8 (18.18) | 11 (25.58) | 0.404 | 0.556 (0.064) |
| Irregular | 3 (6.81) | 21 (48.83) | < 0.001 | 0.713 (0.058) |
| Circumferential | 10 (22.72) | 8 (18.60) | 0.635 | 0.470 (0.064) |
| **Pleural nodule** | 2 (4.54) | 15 (34.88) | < 0.001 | 0.654 (0.061) |
| **Extrapleural fat clouding** | 6 (13.63) | 7 (16.27) | 0.73 | 0.521 (0.064) |

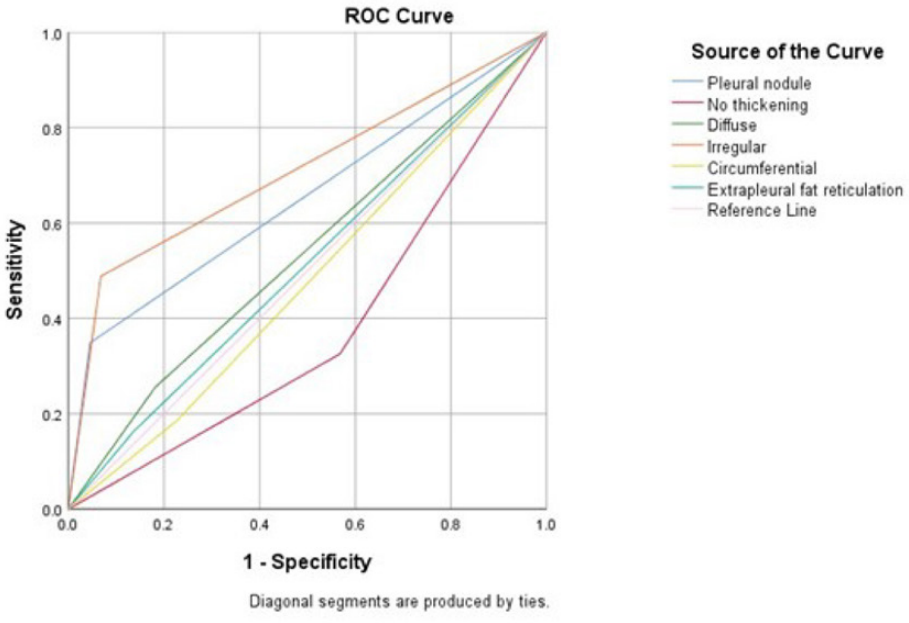


**Figure 6.** *The receiver operating characteristic curves of the associated CT findings for facilitating differentiation between benign and malignant pleural effusions.*

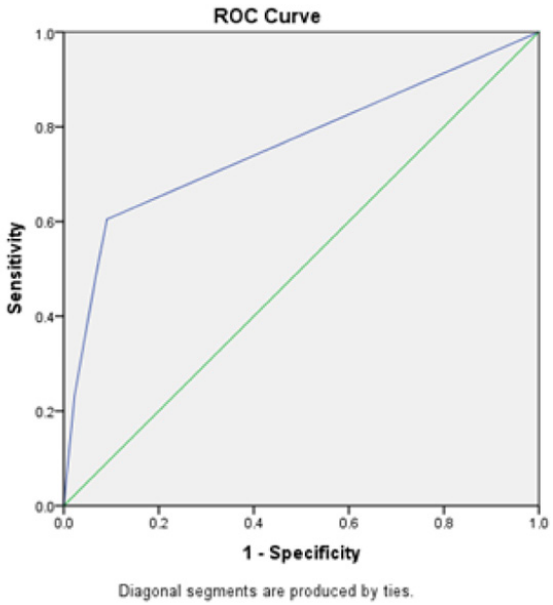


**Figure 7.** *The receiver operating characteristic curve for findings (combining irregular pleural thickening and pleural nodule) facilitating differentiation of malignant pleural effusion from benign pleural effusion (AUC 0.761 and Std. error 0.053).*

## Discussion

In our study, the pleural fluid attenuation values on DECT had no significant role in characterizing pleural effusions as benign or malignant etiologies. The mean CT attenuation values in this study were about the same for both groups of effusion in the standard conventional CT images and even between the monoenergetic images at every energy level. The mean attenuation values ranged from 10-22 HU and did not accurately differentiate between benign and malignant pleural effusions in our study. Some other previous studies also claimed that CT attenuation value was found to be a moderate to poor indicator for characterization of effusions [1, 9]. The increased attenuation of the effusion potentially depends on the levels of protein, lactate dehydrogenase (LDH), bilirubin, haemocytes and hemoglobin which are the more prevalent components of malignant effusions in comparison

THE ASEAN JOURNAL OF RADIOLOGY
ISSN 2672-9393

with benign effusions [10]. However, some benign effusions such as the tuberculous effusions are commonly exudates and invariably contain protein concentrations >30 g/L in up to 77% of cases. Additionally, The LDH level of tuberculous pleural fluid is elevated in approximately 75% of cases, with levels frequently exceeding 500 IU/L [11]. Hamm et. al. [12] found that the elevated pleural cholesterol in malignant effusions is possible due to major cellular degeneration or increased pleural permeability. Consequently, the high cholesterol level, which reduces the attenuation may degrade the expected high CT attenuation values in malignant effusions. These lead us to infer that no significant difference of the mean attenuation values between benign and malignant effusions because of the overlapping attenuation values. However, Zhang et. al. [3] reported that CT attenuation values between the benign and malignant pleural effusions were statistically different in 40keV and 100keV monoenergetic spectral images (43.15±3.79HU vs. 39.42±2.60HU at 40keV, $p = 0.005$; 9.11±1.38HU vs. 6.52±2.04HU at 100keV, $p<0.001$). One possible explanation may be due to the small sample of patients in the study (14 patients with benign pleural effusion and 15 patients with malignant pleural effusion). The mean attenuation values of their study were notably similar in both groups of effusion, which means it would be difficult to apply the findings of these examinations in the clinical use of CT numbers to differentiate pleural fluid.

Z-effective images are the color-coded images based on the effective atomic number of tissues. The coefficients of the photoelectric and Compton scatter components computed during the spectral decomposition process are as a result of influences of the spatial distribution of tissues [13]. The effective atomic number provides a better discrimination than the attenuation values because it displays the material make-up of each pixel [14]. However, our study revealed almost identical effective atomic numbers and iodine concentrations between malignant and benign effusions. These show a correlation with the results of the CT attenuation value and may imply that there is no association between the effective atomic number or the iodine concentration and the type of pleural effusions.

Many studies have proposed that the conventional chest CT can be used to differentiate between benign and malignant pleural effusions by using the imaging characteristics such as pleural nodularity, pleural nodules and pleural thickening [15-20]. Our study found that irregular pleural thickening and pleural nodules were detected at a statistically significant level in the patients with malignant pleural effusions, (48.83%; $p < 0.001$ and 34.88%; $p < 0.001$ respectively). However, the overall accuracy of the use of irregular pleural thickening and pleural nodule to differentiate between benign and pleural effusions was only moderate (AuROC 0.713 and 0.654, respectively). Overall, these findings are in accordance with findings reported by Yilmaz U et. al. [17] who reviewed 146 patients with proven pleural disease. This team reported that pleural nodularity and irregular pleural thickening greater than 1 cm were helpful in distinguishing malignant from benign pleural diseases. The findings of this study are similar to those reported by Leung et. al. [18] which published that nodular pleural thickening had a high specificity (94%) for the diagnosis of malignant pleural disease. A study by Maffessanti et. al. [21] suggested that the absence of pleural thickening does not preclude malignant effusion because 7 out of 12 patients with malignant effusions in that series had normal-appearing pleura. Similar to these findings is our study which found that about one-third of the malignant group had no pleural thickening.

There were some limitations to our study. First, it is retrospective in nature; therefore, the data may not be as standardized as other types of study, and the thoracentesis and DECT were not performed at the same time in some patients. Second, we defined the mean HU using only three axial slices despite the variation in the volume of fluid. It is possible that volume averaging might play a larger role in smaller effusions making attenuation values less accurate. Finally, we determined the results from only one CT scanner vendor's hardware and software application.

## Conclusion

In conclusion, dual-energy spectral CT attenuation values did not demonstrate reliable clinical values in enabling the differentiation between benign and malignant pleural effusions. Associated pleural CT appearance features including pleural nodule and irregular pleural thickening would suggest malignant pleural effusion with moderate accuracy.

## References

1. Abramowitz Y, Simanovsky N, Goldstein MS, Hiller N. Pleural effusion: characterization with CT attenuation values and CT appearance. AJR Am J Roentgenol 2009;192:618-23. doi: 10.2214/AJR.08.1286.

2. Cullu N, Kalemci S, Karakas O, Eser I, Yalcin F, Boyaci FN, et al. Efficacy of CT in diagnosis of transudates and exudates in patients with pleural effusion. Diagn Interv Radiol 2014;20:116-20. doi: 10.5152/dir.2013.13066.

3. Zhang X, Duan H, Yu Y, Ma C, Ren Z, Lei Y, et al. Differential diagnosis between benign and malignant pleural effusion with dual-energy spectral CT. PLoS One 2018;13:e0193714. doi: 10.1371/journal.pone.0193714.

4. Porcel JM, Pardina M, Bielsa S, González A, Light RW. Derivation and validation of a CT scan scoring system for discriminating malignant from benign pleural effusions. Chest2015;147:513-9. doi: 10.1378/chest.14-0013.

5. Basso SMM, Lumachi F, Del Conte A, Sulfaro S, Maffeis F, Ubiali P. Diagnosis of Malignant Pleural Effusion Using CT Scan and Pleural-Fluid Cytology Together. A Preliminary Case-Control Study. Anticancer Res 2020;40:1135-9. doi: 10.21873/anticanres.14054.

6. Silva AC, Morse BG, Hara AK, Paden RG, Hongo N, Pavlicek W. Dual-energy (spectral) CT: applications in abdominal imaging. Radiographics 2011;31:1031-46; discussion 47-50. doi: 10.1148/rg.314105159.

7. Han D, Ma G, Wei L, Ren C, Zhou J, Shen C, et al. Preliminary study on the differentiation between parapelvic cyst and hydronephrosis with non-calculous using only pre-contrast dual-energy spectral CT scans. Br J Radiol 2017;90:20160632. doi: 10.1259/bjr.20160632.

8. Wannasopha Y, Leesmidt K, Srisuwan T, Euathrongchit J, Tantraworasin A. Value of low-keV virtual monoenergetic plus dual-energy computed tomographic imaging for detection of acute pulmonary embolism. PLoS One 2022;17:e0277060. doi: 10.1371/journal.pone.0277060.

9. Nandalur KR, Hardie AH, Bollampally SR, Parmar JP, Hagspiel KD. Accuracy of computed tomography attenuation values in the characterization of pleural fluid: an ROC study. Acad Radiol 2005;12:987-91. doi: 10.1016/j.acra.2005.05.002.

10. Wang M, Zhang Z, Wang X. Superoxide dismutase 2 as a marker to differentiate tuberculous pleural effusions from malignant pleural effusions. Clinics (Sao Paulo) 2014;69:799-803. doi: 10.6061/clinics/2014(12)02.

11. Ferrer J. Tuberculous pleural effusion and tuberculous empyema. Semin Respir Crit Care Med 2001;22:637-46. doi: 10.1055/s-2001-18800.

12. Hamm H, Brohan U, Bohmer R, Missmahl HP. Cholesterol in pleural effusions. A diagnostic aid. Chest 1987;92:296-302. doi: 10.1378/chest.92.2.296.

13. Rassouli N, Etesami M, Dhanantwari A, Rajiah P. Detector-based spectral CT with a novel dual-layer technology: principles and applications. Insights Imaging 2017;8:589-98. doi: 10.1007/s13244-017-0571-4.

14. Alvarez RE, Macovski A. Energy-selective reconstructions in X-ray computerized tomography. Phys Med Biol 1976;21:733-44. doi: 10.1088/0031-9155/21/5/002.

15. Arenas-Jiménez J, Alonso-Charterina S, Sánchez-Payá J, Fernández-Latorre F, Gil-Sánchez S, Lloret-Llorens M. Evaluation of CT findings for diagnosis of pleural effusions. Eur Radiol 2000;10:681-90. doi: 10.1007/s003300050984.

16. Kim KW, Choi HJ, Kang S, Park SY, Jung DC, Cho JY, et al. The utility of multi-detector computed tomography in the diagnosis of malignant pleural effusion in the patients with ovarian cancer. Eur J Radiol 2010;75:230-5. doi: 10.1016/j.ejrad.2009.04.061.

17. Yilmaz U, Polat G, Sahin N, Soy O, Gülay U. CT in differential diagnosis of benign and malignant pleural disease. Monaldi Arch Chest Dis 2005;63:17-22. doi: 10.4081/monaldi.2005.653.

18. Leung AN, Müller NL, Miller RR. CT in differential diagnosis of diffuse pleural disease. AJR Am J Roentgenol 1990;154:487-92. doi: 10.2214/ajr.154.3.2106209.

19. Traill ZC, Davies RJ, Gleeson FV. Thoracic computed tomography in patients with suspected malignant pleural effusions. Clin Radiol 2001;56:193-6. doi: 10.1053/crad.2000.0573.

20. Aquino SL, Webb WR, Gushiken BJ. Pleural exudates and transudates: diagnosis with contrast-enhanced CT. Radiology 1994;192:803-8. doi: 10.1148/radiology.192.3.8058951.

21. Maffessanti M, Tommasi M, Pellegrini P. Computed tomography of free pleural effusions. Eur J Radiol 1987;7:87-90.

ASEAN Movement in Radiology

# Asian Radiology Education Program (AREP): A new step of radiology education in Asia

*Silanath Terpenning, MD.*
*Janardhana Ponnatapura, M.D.*
From Department of Radiology, Atrium Health Wake Forest Baptist,Wake Forest University School of Medicine, Winston-Salem, North Carolina, USA.
Address correspondence to S.T. (email: natsawadee@yahoo.com)

Received 21 September 2022 ; accepted 5 Octorber 2022
doi:10.46475/aseanjr.v23i3.186

**Keywords:** Radiology education, Asia, Non-profit, Wake Forest University School of Medicine, AREP, Asian Radiology Education Program.

It is an honor for me to write this article about the ASEAN Movement in Radiology. Almost 20 years ago while I was a junior staff at Siriraj Hospital, Mahidol University in Bangkok, Thailand, I had two articles published in The ASEAN Journal of Radiology and I still keep the hard copies with me even now.

I am grateful to both Thailand and USA for providing me with an excellent training in radiology. Throughout my training and career in Thailand and USA, I have always been motivated to pay back to our radiology society.

My colleague, Dr. Janardhana Ponnatapura, an Assistant Professor in Cardiothoracic Imaging and Section Chief, Department of Radiology, Atrium Health Wake Forest Baptist, Wake Forest University School of Medicine, one of the most remarkable and knowledgeable radiologists has provided his insight below.

“Coming from a medical family background has given me a great exposure in medicine and a profound sense of integrity and responsibility. During my medical school days in India, I frequently saw a lot of patients from neglected sectors of society and was close to the cradle of basic human feelings. After each case, I had to reassess myself both as a clinician striving towards perfection and as a person striving towards empathy for my patients.

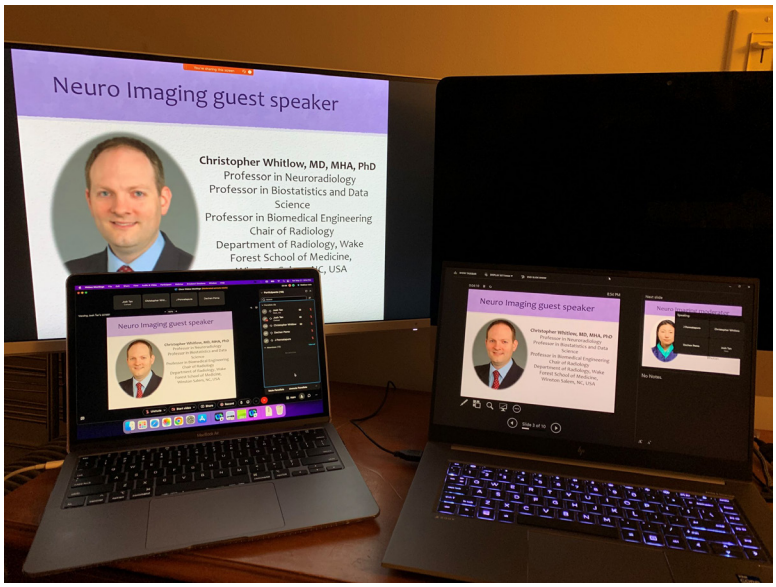



"Vasudhaiva Kutumbakam", a Sanskrit phrase in one of the Hindu texts means "The World Is One Family". One of the meaningful ways to give back to the community is to volunteer your time to support a cause you are passionate about and that which enriches your life, also gives you an opportunity to grow as a person, to better understand how you fit into the world around you. Having a unique opportunity to work in America where there is a strong healthcare system with numerous opportunities for research, and advance technology, I sense it is essential to contribute back to the radiology community".

Most Asian countries have made great advancements in radiology education. Asia hosts several important international meetings annually. We have the newest scanners and well-trained personnel; however, some of our neighbor countries are still struggling to catch up. To assist in the matter, the "Asian Radiology Education Program" was created in October 2021 with collaboration from our volunteer radiology colleagues in Bhutan, Cambodia, Indonesia, Laos, Nepal, Myanmar, Mongolia, Thailand and Vietnam. Our program is a non-profit program, therefore, free of charge.

The purposes of this program are to share experiences, expertise and knowledge from the West to radiology colleagues in Asia and to collaborate research projects, radiology education and exchange visitor programs in the near future.

We broadcast live radiology education webinars three weekends each month with multiple subspeciality lecture series: Cardiothoracic Imaging, Body Imaging, Neuroradiology, MSK Radiology and Hot Topics in Radiology (27 lectures this year in total). This year's program runs from January to September 2022.

Our moderators are academic radiologists from member countries and our guest speakers are from leading academic institutes in the US such as the University of Texas MD Anderson Cancer Center (Houston, TX), the University of Maryland (Baltimore, MD), Emory University School of Medicine (Atlanta, GA), the University of New Mexico (Albuquerque, NM), The Johns Hopkins University (Baltimore, MD), Medical College of Wisconsin (Milwaukee, WI), the University of Texas at San Antonio (San Antonio, TX), the University of Washington (Seattle, WA), NYU Langone Health (New York, NY), the University of Miami Miller School of Medicine (Miami, FL) and Atrium Health Wake Forest Baptist, Wake Forest University School of Medicine (Winston-Salem, NC).

Going forward, we desire to involve more Asian countries to participate in this educational program and develop a strong intent to create an annual outreach program from our institute, where radiology residents from the Wake Forest School of Medicine can rotate in these countries and contribute to the increase of radiology care and access across the globe, and also learn about international healthcare.

Thank you for the opportunity to share a few thoughts about our program. We deliver directly from our hearts to your hearts!

Respectfully,

*Janardhana Ponnatapura, M.D.*
Assistant Professor,
Section Chief and Fellowship Director,
Cardiothoracic Imaging,
Co-Director Asian Radiology Education Program

*Silanath Terpenning, M.D.*
Associate Professor,
Cardiothoracic Imaging,
Director Asian Radiology Education Program

THE ASEAN JOURNAL OF RADIOLOGY
ISSN 2672-9393

ASEAN Movement in Radiology

# MFU Wellness Center and FUJIFILM bring medical innovation to provide people in remote areas of Chiang Rai tuberculosis screening with the aim of reducing limitations to access basic healthcare services

*Saparat Pradith, B.A.*
*Yuva Kaewvises, B.A.*
From FUJIFILM (Thailand) Ltd., 388 S.P. Building, 8th Floor, Phaholyothin Road, Samsennai, Phayathai, Bangkok, Thailand.
Address correspondence to S.P. (saparat.pradith@fujifilm.com)

Received 22 December 2022 ; accepted 22 December 2022
doi:10.46475/aseanjr.v23i3.200

**Keywords:** Tuberculosis, Screening, Remote area, Portable X-ray, Corporate social responsibility.

Mae Fah Luang University (MFU) Wellness Center and FUJIFILM forge a partnership in conducting physical checkups in remote areas of Chiang Rai, including Ban Laolew and Ban Pangmahan with the aim of promoting proactive tuberculosis (TB) screening and reducing limitations to access basic healthcare services among locals, hill tribes and stateless minorities.

Chiang Rai is the northernmost province of Thailand where the borders of Thailand, Laos and Myanmar converge. Ban Laolew and Ban Pangmahan are the geographically remote communities in Chiang Rai which are located uphill and almost a hundred kilometers away from the city center. The locals encountered difficulty in accessing healthcare services and never had a chance to take X-ray due mainly to inaccessibility by an X-ray van. Moreover, it was reported that 67 tuberculosis patients were found in Mae Fah Luang, Chiang Rai in 2021 with 8.95 percent of mortality rate per annum. For this reason, the collaborative partnership

between MFU Wellness Center and FUJIFILM was established to tackle this issue through the integration of MFU Wellness Center's holistic healthcare services, ranging from basic healthcare to complicated medical surgeries, and FUJIFILM's medical innovation, FDR Xair, the portable X-ray unit with the ability to X-ray bedridden patients.

FDR Xair is a compact and portable X-ray unit with only 3.5 kilos in weight. It is suitable for bedridden patient X-ray and mobile checkup in the remote areas where X-ray van cannot access. The X-ray unit provides safe and sufficient radiation dose as recommended by WHO. In addition, the FDR Xair is equipped with AI technology which could transfer X-ray images onto a computer and locate lung abnormalities rapidly and accurately.

In this event, there was a total of 550 people who had registered for the checkup and 147 cases were detected to develop pulmonary-related conditions and were given appointments for treatment in the next step.

**Associate Professor Chayaporn Wattanasiri, Ph.D., President of MFU**, said "MFU was established by the name of the mother of King Rama IX, Her Royal Highness Princess Srinagarindra, who was lovingly known as **Mae Fah Luang**. HRH Princess Srinagarindra lavished her attention upon overall health and well-being of her subjects that contributed to the foundation of the MFU Wellness Center for providing people with basic healthcare services which prevent people from getting sick and reduce the burden on the national health expenditure. To maintain one's good health, the MFU Wellness Center is strongly oriented towards education and disease prevention rather than treatment as it is our mission to achieve sustainable healthcare."

**Assistant Professor Thawatchai Aphidechakul, Dr.P.H., Acting Director of MFU Wellness Center**, added "MFU Wellness center operates its services through 3P strategy: Prediction, Prevention and Promotion, which heavily emphasizes on people who face difficulty in getting medical services. Previously, we came across obstacles to providing mobile checkup and reaching out to TB patients in remote

areas as the equipment that we have cannot be relocated into the areas. Therefore, the physical checkup under the collaboration of the MFU Wellness Center and FUJIFILM, that offers medical equipment support, has allowed medical professionals to provide diagnosis, basic healthcare services, and treatment for people with proper care.

**Mr. Yuto Kumagai, Assistant to Managing Director, FUJIFILM (Thailand) Ltd.,** stated, "As a responsible corporate citizen, Fujifilm is firmly committed to solving social issues in all dimensions, especially health inequality. To solve the issue, we have continuously created and developed our medical innovations and technologies which cover three key health aspects: Prevention, Diagnosis, and Treatment. In this mobile checkup, we are aware of the limitations in terms of access to the remote areas, so we are bringing our medical imaging solution, FDR Xair, to support medical professionals in this physical checkup, relieving burdens on the medical staff's part."

Fujifilm always places strong emphasis on solving social issues, especially health issue that affects not only an individual, but creates negative impacts on the wider society. In 2021, Fujifilm launched its new corporate campaign **"NEVER STOP"** that reinforced its commitment to never stop creating a wide range of innovations and technologies that allow people to live a healthier life and create new values, to give back to society.

ASEAN Movement in Radiology

# The first face-to-face Malaysian Congress of Radiology after the COVID-19 outbreak

*Socheat Chum, M.D.*
From Department of Diagnostic and Interventional Radiology, Calmette Hospital, Phnom Penh, Cambodia.
Address correspondence to S.C. (chumsocheatmd@gmail.com)

Received 28 December 2022 ; accepted 28 December 2022
doi:10.46475/aseanjr.v23i3.202

**Keywords:** Malaysian Congress of Radiology, COVID-19.

The Malaysian Congress of Radiology (MCOR) returned to its in-person form this year in the beautiful city of Penang, 7-9 December 2022 alongside the launching of the Malaysian Society of Radiologists (MYRAD). As an international delegate from Cambodia, it was my great privilege to attend this event which I found educational and inspiring.


*(Right) The author and (Left) Associate Professor Wiwatana Tanomkiat, the President of the Royal College of Radiologists of Thailand (RCRT) and Professor Norlisah Mohd Ramli, the President of the College of Radiology (CoR), Academy of Medicine of Malaysia, at MCOR.*

THE ASEAN JOURNAL OF RADIOLOGY
ISSN 2672-9393

The majority of the presenters were local Malaysians speaking fluent English and delivered a comprehensive review and update of various subspecialties in diagnostic radiology. I witnessed a great lecture of Dr. Norzaini Rose Mohd Zain on the imaging approach of Alzheimer's disease, and an inspiring lecture by Professor Kartini Rahmat on Artificial Intelligence (AI) in breast imaging, turning complexities into simple practical solutions. There was something for just about everyone: diagnostic radiology and intervention, research, artificial intelligence (AI) and so on. The participants were so interactive and dynamic, relentlessly asking questions in each session. A young radiologist like myself would love the beauty and inspiration of the quiz sessions, lectures on oncologic imaging, and tips on board examination preparation.


*Professor Kartini Rahmat, the Organizing Chair of MOCR2022, thanks her faculty members in the MCOR Faculty Appreciation dinner.*

The hospitality of Malaysian people is impressive. I felt part of in the congress. From the moment I first entered the venue, I was greeted and guided cordially to foods, culture, city sightseeing and history.

I formed new friendships and networking quickly and effortlessly, from exchanging our cultures to sharing experiences and challenges in our current practice. Finally, I would like to extend my gratitude to the organizing committee of MCOR for the efforts to produce such an exciting event. I recommend our ASEAN colleagues without any hesitation to participate in the upcoming Malaysian radiological event.

# ASEAN JOURNAL OF RADIOLOGY

**This journal provide 4 areas of editorial services: language editing, statistical editing, content editing, and complete reference-citation check in 8 steps:**

| Step | Services to authors | Services providers |
|---|---|---|
| I | Manuscript submitted | Editor |
| II | Language editing/ A reference-citation check | Language consultant/Bibliographer |
| III | First revision to ensure that all information remains correct after language editing | Editor |
| IV | Statistical editing | Statistical consultant |
| V | Content editing* | Three reviewers |
| VI | Second revision | Editor |
| VII | Manuscript accepted/ rejected | Editor/Editorial board |
| VIII | Manuscript published | Editorial office |

*Content editing follows a double-blind reviewing procedure